International Journal of Civil Engineering (2023) 21:1315–1342
https://doi.org/10.1007/s40999-023-00845-1

RESEARCH PAPER

Numerical Investigation on the Fire Resistance of Partially Encased Steel Columns

Ricardo A. Hoffstaeter[1] · Paulo A. G Piloto[2] · Carlos Humberto Martins[3] · Ronaldo Rigobello[4]

Received: 21 December 2022 / Revised: 1 May 2023 / Accepted: 7 May 2023 / Published online: 19 May 2023

Abstract

This paper presented the results of numerical analyses on the fire resistance of composite columns with partially encased steel columns (PEC). This investigation used 2D and 3D finite element models and assessed for the design method of composite elements under compression according to the Annex G of Eurocode 4. New proposals were presented to determine the buckling resistance of PEC under standard fire. The 2D and 3D numerical models were based on American and European steel profiles. The 2D thermal model was used to improve the design method of the current version of the Eurocode 4, enhancing the balance summation model, which is currently used to determine the plastic resistance to axial compression and the effective flexural stiffness of the four components of the cross-section. The 3D thermomechanical model used the temperature field for each fire rating time (30, 60, 90, and 120 min) and applied the incremental load step solution method, based on the Newton–Raphson, to determine the buckling load of partially encased columns with 3 and 5 m, considering different supporting conditions. These results present a safer buckling curve when compared to curve "c".

Keywords Partially Encased Columns · Fire Resistance · Buckling resistance

List of symbols

A_c	Concrete cross-sectional area
A_s	Cross-sectional area of the reinforcinbars
$A_{s,\theta}$	Cross-sectional area of the reinforcing bars at elevated temperatures
A_w	Cross-sectional area of a steel web
E	Characteristic value for the modulus of elasticity
E_a	Characteristic value for the modulus of elasticity of structural steel at 20 °C
E_s	Modulus of elasticity of the reinforcing bars at 20 °C
$E_{a,\theta}$	Characteristic value for the slope of the linear elastic range of the stress–strain relationship of structural steel at elevated temperatures
$E_{s,\theta}$	Characteristic value for the slope of the linear elastic range of the stress-strainrelationship of reinforcing steel at elevated temperatures
E_{cm}	Secant modulus of elasticity of concrete
$E_{c,sec,\theta}$	Characteristic value for the secant modulus of concrete in the fire situation, Given by $f_{c,\theta}/\varepsilon_{c,sec,\theta}$
$(EI)_{fi,eff,z,}$	Flexural stiffness in the fire situation
$(EI)_{fi,eff,z,f}$	Flexural stiffness of the flanges in the fire situation
$(EI)_{fi,eff,z,w}$	Flexural stiffness of the web in the fire situation
$(EI)_{fi,eff,z,c}$	Flexural stiffness of the concrete in the fire situation
$(EI)_{fi,eff,z,s}$	Flexural stiffness of the reinforcing bars in the fire situation
H_t	Parameter for height reduction of the web
I_z	Second moment of area of the cross-section for bending around the weak axis in the fire situation

✉ Carlos Humberto Martins
chmartins@uem.br

[1] Department of Civil Engineering, State University of Maringá, Colombo Av, Maringá, Paraná 5790, Brazil

[2] INEGI-LAETA, Instituto Politécnico de Bragança, Bragança, Portugal

[3] Department of Civil Engineering, State University of Maringá, Colombo Av, Maringá, Paraná 5790, Brazil

[4] Federal University of Technology - Paraná, Campo Mourão, Paraná, Brazil

$I_{s,\theta}$	Second moment of area of the reinforcing bars for bending around the weak axis in the fire situation
L	Reference length of a column
L_{fi}	Buckling length of a column
$N_{fi,Rd}$	Design value of the resistance of a member in axial compression in the fire situation
$N_{fi,cr,z}$	Elastic critical load in the fire situation
$N_{fi,pl,Rd}$	Design value of the plastic resistance to axial compression of the total cross-section in the fire situation
$N_{fi,pl,Rd,f}$	Design value of the plastic resistance to axial compression of the flanges in the fire situation
$N_{fi,pl,Rd,w}$	Design value of the plastic resistance to axial compression of the web in the fire situation
$N_{fi,pl,Rd,c}$	Design value of the plastic resistance to axial compression of the concrete in the fire situation
$N_{fi,pl,Rd,s}$	Design value of the plastic resistance to axial compression of the reinforcing bars in the fire situation
b_c	Width of the partially encased column
$b_{c,fi,h}$	Horizontal width reduction of the encased concrete
$b_{c,fi,v}$	Vertical width reduction of the encased
d_c	Height of the partially encased column
f_{ck}	Characteristic value for the compressive cylinder strength of concrete
$f_{c,\theta}$	Mean value of axial tensile strength of concrete in the fire situation
f_{ay}	characteristic or nominal value for the yield strength of structural steel at 20 °C
f_{sy}	characteristic or nominal value for the yield strength of reinforcing steel at 20 °C
$f_{sy,\theta}$	Maximum stress level or effective yield strength of reinforcing steel in the firesituation
$h_{w,fi}$	Reduction in the height of the metal profiles web
$k_{IM,t}$	Empirical coefficient related to the section factor
$k_{f,t}$	Empirical coefficient related to the thickness of the steel profile flange
$k_{w,t}$	Empirical coefficient related to the thickness of the steel profile web
$k_{s,t}$	Empirical coefficient related to reinforcing bars
$k_{b0,t}$	Empirical coefficient of a reference distance
$k_{Ac,t}$	Empirical coefficient related to the concrete area
$k_{bc,t}$	Empirical coefficient related to steel profile width
$k_{E,\theta}$	Reduction factor for the modulus of elasticity of steel at temperature θ
t	Fire exposure time
t_f	Thickness of the flange of the steel profile
t_w	Thickness of the web of the steel profile
$(u/A)_p$	Section Factor
u_s	Geometrical average of the axis distances u1 and u2
u_1	The axis distance from the outer reinforcing bar to the inner flange edge
u_2	The axis distance from the outer reinforcing bar to the concrete surface
α	Imperfection factor for buckling curves
αc	convective heat transfer coefficient
$\gamma_{M,fi,a}$	partial factor for the strength of structural steel in the fire situation
$\gamma_{M,fi,c}$	partial factor for the strength of concrete in the fire situation
$\gamma_{M,fi,s}$	partial factor for the strength of reinforcing bars in the fire situation
ϕ	Diameter of the reinforcing bar
$\theta_{f,t}$	Average temperature of flanges of the steel profile
$\theta_{w,t}$	Average temperature of web of the steel profile
$\theta_{c,t}$	Average temperature of concrete
$\theta_{s,t}$	Average temperature of reinforcing bars
$\theta_{0,t}$	Temperature reference value in a period of exposure to fire
$\overline{\lambda}_{\theta,fi}$	Non-dimensional slenderness ratio in the fire situation
$\chi_{f,i}$	Reduction factor due to flexural buckling in the fire situation

1 Introduction

Concrete and steel are the most used materials in civil construction. Urban and economic development in the world today is so significant that it would be impossible to imagine everyday life without the use of these materials [1, 2].

Partially encased steel columns (PEC) are usually made of hot-rolled steel profiles reinforced with concrete between the flanges. The composite section is responsible for increasing the torsional and bending stiffness without increasing the section dimension when compared to the same cross-section of steel profile, being the concrete portion very significant to increase the fire resistance [3].

Since the thermal conductivity of concrete is relatively small, the temperature field in the composite cross-section is highly non-uniform. There isn't a simplified method is available to solve the heat transfer analysis; therefore, a numerical simulation is required to analyze the fire effect. The current design standard in Europe is included in the [4] that presents the balanced summation model for calculating the fire resistance of PEC for bending around the weak axis when exposed to fire all around the column, according to the standard temperature–time curve [5].

In the last century, research involving the safety of structures has been among the main concerns of both designers and policymakers. [6] and [7] evaluated the effects of high temperatures on concrete columns. Later, in 1978, [8] proposed a simplified method, called the isotherm method of 500 °C, considering the cross-section under fire.This method assumes that concrete with temperatures higher than 500 °C is disregarded for the load-bearing capacity. In this way, the concrete of this inner region is considered with the original properties at room temperature. Other important research about composite section profiles on structural elements that stand out were [9, 10], in addition to the study in [11].

In [12], the authors conducted a comprehensive study of cast iron columns' behavior and fire resistance based on numerical simulations using ABAQUS software. The numerical model was validated against six fire tests and then used to investigate the effects of several parameters (column slenderness, load factor, load eccentricity, imperfections of columns, cross-section, and axial restraint) on column behavior cast iron under fire. The parametric analysis results indicate that the applied load governs the fire resistance, and these columns are sensitive to load eccentricity. Based on the comparison between numerical simulation results, the authors concluded that the method in [13] provides a safe and reasonably accurate estimation of cast iron columns' strength and fire resistance.

[13] and [14] are examples of other experimental studies on composite columns in fire conditions that should be highlighted for evaluating the performance of these elements at high temperatures. In 2006 [15] developed experimental tests on built-up PEC with high and normal-strength concrete at room temperature. High-strength specimens concrete had a more brittle failure mode than normal-strength concrete; however, this situation was overcome by introducing steel fibers. The study developed by [16] in 2006, presented a new design concept called the residual area method to calculate the equivalent thickness of concrete for temperature analysis of concrete-encased I-sections in fire. The design of the equivalent concrete thickness was based on a regression analysis which is verified by experimental results. The proposed method makes use of the Eurocode 3 provisions to formulate the temperature response of each representative point along the steel profile using a 1D heat transfer model. The proposed method is applied to concrete-encased I-sections exposed to hydrocarbon, external and parametric fire curves. The results demonstrated that the residual area method is intrinsic to the geometric configurations (cross-sections) of concrete-encased I-sections, but independent of heating conditions.

Another relevant experimental and numerical study on composite columns in fire situations was developed in [17]. [16] presented an experimental study of PEC with restraining to thermal elongation, [18] in 2010 concluded that the [4] was conservative for all the concrete-encased steel composite columns with some exceptions. In [19], the authors developed experimental tests to show how the building structure influences the performance of PEC when subjected to fire.

[20] carried out an experimental and analytical study on the load capacity of reinforced concrete (RC) columns under the effect of high temperatures. The authors concluded that the initial stiffness of RC columns with a circular cross-section exposed to 500 °C was 13 times lower than that of unexposed RC columns. Thus, the authors proposed an analytical model to predict RC columns' residual axial load-carrying capacity.

[21] investigated the fire resistance of concrete-encased steel (CES) composite columns produced with high-strength concrete (C120) and high-strength steel (S500/S690). The same authors, in [22] proposed two solution methods, one based on an artificial neural network (ANN) and the other using analytical equations, to predict the fire resistance of axially-loaded CES columns made of high-strength concrete. The authors concluded that the ANN and the analytical equations provided results accurate results to the fire resistance values for these CES columns; and recommend modifying the current fire-resistant design methods of CES columns made of high-strength concrete.

In [23], the authors performed an interesting case study on the structural response ina 16-storybuilding affected by a fire.They conclude that columns involved by a layer of masonry resisted the fire and that failure started in the ceiling trusses.

Other studies have been carried out to improve the design procedures presented in [4], in particular the fire resistance of partially encased beams, the resistance to compression, and the effective flexural stiffness of PECunder fire, following the works developed in [24–27]. More recently, [28] concluded that the load-bearing capacity of the composite columns reduces significantly with eccentric loading under fire and increases when PEC changed from two exposed sides to four exposed sides.

The fire resistance of PEC depends on the temperature evolution during fire exposure. This study aims to evaluate the Balanced Summation Method's effect on PEC's flexural buckling design. The 2D analysis is devoted to improving the calculation of the axial buckling load at elevated temperatures, particularly the plastic resistance to axial compression and the effective flexural stiffness of the cross-section. New formulations are proposed to calculate the average temperature of the cross-section on the four components of PEC improving the accuracy, and suggesting modifications to Annex G of [4]. The simplified method is based on new formulations for specific fire ratings R30, R60, R90, and R120 when submitted to the standard fire curve [5]. New formulations are presented to determine the average temperature of the flanges, the average temperature of the web, the residual areaand the average temperature of concrete, and the average temperature of the reinforcements.

This research also proposes a new imperfection factor (buckling curve) for the reduction factor associated with the buckling resistance of PEC under standard fire curve [5]. This proposal uses a Geometrically and Material Non-Linear Imperfection Analysis (GMNIA) on a full 3D finite element model.

In this context, the present work aims to enhance thesimplified method used to determine the axial buckling resistance of PEC under fire, proposing new formulas and coefficients for a wide spectrum of structural steel profiles.

2 Materials and Methods

The finite element software ANSYS was used for the nonlinearsolution of the 2D thermal analysis of the PEC cross-section and the non-linear thermo-mechanical solution of the 3D PEC model. The 2D numerical results of the temperature evolution of the cross-section were obtained through an incremental solution time, withan iterative process regarding the temperature dependence of the materials involved. At first, the 2D numerical models were developed to determine the temperature field in the 42 selected steel sections for each required fire rating time of 30, 60, 90, and 120 min. With these results, a new formulation is presented to determine the average temperature in the four components of the cross-section improving the current proposal of [4].The 3D numerical models belong to the second phase of this research and include four solution steps.The first step consisted of the thermal analysis based on the non-linear solution to determine the temperature field from a shorter number of the 22 composite columns under fire for each fire rating time of 30, 60, 90, and 120 min. This temperature field has been used in a different step process for the mechanical analysis, as a nodal thermal load. The second step was the elastic buckling analysis to determine the critical load and mode of instability, using the 22-section profiles for each of the three bending conditions and the two lengths (3 and 5 m). The third step consisted of the GMNIA model to find the plastic resistance to axial compressionin the fire situation, assuming the same material model behaviour in the four required fire ratings. Both steps 2 and 3 could have been developed using simple calculation methods, but it was decided to use the results from the numerical analysis.The fourth step consisted of the GMNIA model to find the buckling load under fire for each fire rating, column length, and end condition.

Tables 1 and 2 present the principal dimensions and characteristics of the cross-sections studied the number of reinforcing bars, their respective diameters, concrete covering thickness, and section factors.

The mechanical properties used for the materials following the European standard are present in Table 3 at room temperature.

The European standard [29] defines the reduction factors for the mechanical properties of hot-rolled steel. [30] defines the reduction factors for mechanical characteristics of concrete at elevated temperatures.

3 New Proposal

The [2] defines, for the design buckling resistance of PEC, the value of the plastic resistance to axial compression and the value of the effective flexural stiffness under fire conditions. The simplified calculation method was initially developed by [31] to calculate the fire resistance of the partially encased columns, dividing the cross-section into four components: flanges, web, reinforcing bars, and concrete, according to Fig. 1.

The current design method, defined in[4] complies with the corresponding principlesand is based on simple formulas and empirical coefficients,which appeared to be unsafe. Unsafe means over-predicting the components' temperature, as demonstrated by the 2D analysis and over-predicting the buckling resistance, as demonstrated by the 3D analysis. Each component should be evaluated based on the evolution of its temperature and its effect on the yield strength and the modulus of elasticity. The design value of the plastic resistance to axial compression and the effective flexural stiffness of the cross-section was obtained by the balanced summation model. Steel and concrete's strength and deformation properties at elevated temperatures were according to material models presented in [29] and [30]. The design buckling resistance for composite columns under fire, $N_{fi,Rd}$, requires the calculation of the plastic

Table 1 Characteristics of the Americansteel sections under study

Profiles	$(u/A)_p$ [m^{-1}]	t_w [mm]	t_f [mm]	b_c [mm]	d_c [mm]	n° r.b	ϕ [mm]	u_1 [mm]	u_2 [mm]	$\frac{A_s}{A_s+A_c}$	$\frac{t_w}{t_f}$
HP 250 × 62.0 (H)	15.94	10.5	10.7	256.0	246.0	4	20	50	50	2.28%	0.98
HP 250 × 85.0 (H)	15.57	14.4	14.4	260.0	254.0	4	20	50	50	2.27%	1.00
HP 310 × 79.0 (H)	13.22	11.0	11.0	306.0	299.0	4	25	50	50	2.40%	1.00
HP 310 × 93.0 (H)	13.09	13.1	13.1	308.0	303.0	4	25	50	50	2.41%	1.00
HP 310 × 110.0 (H)	12.95	15.4	15.5	310.0	308.0	4	32	50	50	3.94%	0.99
HP 310 × 125.0 (H)	12.82	17.4	17.4	312.0	312.0	4	32	50	50	3.94%	1.00
HP 310 × 132 (H)	12.76	18.3	18.3	313.0	314.0	4	32	50	50	3.94%	1.00
W 250 × 73.0 (H)	15.78	8.6	14.2	254.0	253.0	4	25	50	50	3.56%	0.61
W 250 × 80.0 (H)	15.66	9.4	15.6	255.0	256.0	4	25	50	50	3.56%	0.60
W 250 × 89.0 (H)	15.50	10.7	17.3	256.0	260.0	4	25	50	50	3.55%	0.62
W 250 × 101.0 (H)	15.36	11.9	19.6	257.0	264.0	4	25	50	50	3.56%	0.61
W 250 × 115.0 (H)	15.16	13.5	22.1	259.0	269.0	4	25	50	50	3.56%	0.61
W 310 × 97.0 (H)	13.05	9.9	15.4	305.0	308.0	4	32	50	50	3.93%	0.64
W 310 × 107.0 (H)	12.97	10.9	17.0	306.0	311.0	4	32	50	50	3.94%	0.64
W 310 × 117.0 (H)	12.88	11.9	18.7	307.0	314.0	4	32	50	50	3.94%	0.64
W 310 × 129.0 (H)	12.78	13.1	20.6	308.0	318.0	4	32	50	50	3.94%	0.64
W 360 × 91.0 (H)	13.54	9.5	16.4	254.0	353.0	4	32	50	50	4.11%	0.58
W 360 × 101.0 (H)	13.45	10.5	18.3	255.0	357.0	4	32	50	50	4.11%	0.57
W 360 × 110.0 (H)	13.37	11.4	19.9	256.0	360.0	4	32	50	50	4.11%	0.57
W 360 × 122.0 (H)	13.29	13.0	21.7	257.0	363.0	4	32	50	50	4.13%	0.60
W 410 × 46.1	19.25	7.0	11.2	140.0	403.0	4	20	50	50	2.48%	0.63
W 410 × 53.0	16.26	7.5	10.9	177.0	403.0	4	25	50	50	3.04%	0.69
W 410 × 60.0	16.15	7.7	12.8	178.0	407.0	4	25	50	50	3.02%	0.60
W 410 × 75.0	15.95	9.7	16.0	180.0	413.0	4	25	50	50	3.03%	0.61
W 410 × 85.0	15.85	10.9	18.2	181.0	417.0	4	25	50	50	3.03%	0.60
W 460 × 52.0	17.60	7.6	10.8	152.0	450.0	4	25	50	50	3.17%	0.70
W 460 × 68.0	17.34	9.1	15.4	154.0	459.0	4	25	50	50	3.16%	0.59
W 460 × 82.0	14.82	9.9	16.0	191.0	460.0	4	32	50	50	4.15%	0.62
W 460 × 97.0	14.65	11.4	19.0	193.0	466.0	4	32	50	50	4.14%	0.60
W 460 × 106.0	14.57	12.6	20.6	194.0	469.0	4	32	50	50	4.15%	0.61
W 530 × 66.0	15.93	8.9	11.4	165.0	525.0	4	32	50	50	4.10%	0.78
W 530 × 74.0	15.83	9.7	13.6	166.0	529.0	4	32	50	50	4.10%	0.71
W 530 × 85.0	15.79	10.3	16.5	166.0	535.0	4	32	50	50	4.12%	0.62
W 530 × 92.0	13.32	10.2	15.6	209.0	533.0	4	32	50	50	3.22%	0.65
W 530 × 101.0	13.25	10.9	17.4	210.0	537.0	4	32	50	50	3.22%	0.63
W 530 × 109.0	13.19	11.6	18.8	211.0	539.0	4	32	50	50	3.22%	0.62
W 610 × 125.0	12.00	11.9	19.6	229.0	612.0	4	40	50	50	4.04%	0.61
W 610 × 140.0	11.94	13.1	22.2	230.0	617.0	4	40	50	50	4.05%	0.59
W 610 × 155.0	9.45	12.7	19.0	324.0	611.0	4	40	50	50	2.82%	0.67
W 610 × 174.0	9.40	14.0	21.6	325.0	616.0	4	40	50	50	2.82%	0.65
W 610 × 195.0	9.33	15.4	24.4	327.0	622.0	4	40	50	50	2.81%	0.63
W 610 × 217.0	9.28	16.5	27.5	328.0	628.0	4	40	50	50	2.82%	0.60

Table 2 Characteristics of the European steel sections under study

Profiles	$(u/A)_p$ [m^{-1}]	t_w [mm]	t_f [mm]	b_c [mm]	d_c [mm]	n° r.b	ϕ [mm]	u_1 [mm]	u_2 [mm]	$\frac{A_s}{A_s + A_c}$	$\frac{tw}{t_f}$
HEB200	20.00	9.0	15.0	200	200	4	20	50	50	3.87%	0.60
HEB220	18.18	9.5	16.0	220	220	4	25	50	50	4.96%	0.59
HEB240	16.67	10.0	17.0	240	240	4	25	50	50	4.14%	0.59
HEB260	15.38	10.0	17.5	260	260	4	32	50	50	5.72%	0.57
HEB280	14.29	10.5	18.0	280	280	4	32	50	50	4.89%	0.58
HEB300	13.33	11.0	19.0	300	300	4	32	50	50	4.25%	0.58
HEB320	12.92	11.5	20.5	300	320	4	32	50	50	4.00%	0.56
HEB340	12.55	12.0	21.5	300	340	4	40	50	50	5.88%	0.56
HEB360	12.22	12.5	22.5	300	360	4	40	50	50	5.55%	0.56
HEB400	11.67	13.5	24.0	300	400	4	40	70	50	4.98%	0.56
HEB450	11.11	14.0	26.0	300	450	4	40	70	50	4.42%	0.54
HEB500	10.67	14.5	28.0	300	500	4	40	70	50	3.97%	0.52

resistance to axial compression $N_{fi,pl,Rd}$, the calculation of the elastic critical load under fire $N_{fi,cr,z}$. This elastic critical load depends on the effective flexural stiffness around the weak axis of the cross-section.$(EI)_{fi,eff,z}$. The strength classes of materials and their mechanical and thermal properties were used as parameters to calculate the load-bearing capacity of PEC under fire. The new proposal is presented in the following sections. The results of the thermal and mechanical models were validated with experimental results [28]. Thus the new proposal should accurately predict the real temperatures of the components and the deformation at elevated temperatures.

3.1 Flanges of the Steel Profile

A new formulation is presented for calculating the average temperature on the flanges, Eq. 1, where a new parameter was introduced for the agreement between the numerical results with the new proposal. The 2D numerical results from the thermal analysis were used to determine the average temperature of the flanges for each fire rating time. The average flange temperature from the 42 Brazilian cross-sections was compared with that of the European profiles [25–27]. The database used to calculate the average temperature of the flange was formed by 83 different types of cross-Sects. (42 American and 41 European). However, when using some differentconcrete cover dimensions (u_1 and u_2 parameters) for the same cross-section, 123 different cross-sections were analyzed. The general conditions of the applicability limit of this design step are the PEC exposed to standard fire [5] on all sides, with the conditions of having a section factor greater than 9.0 [m^{-1}] and the thickness of the flanges less than 30 [mm]. With the applicability limit presented here in for commercial steel profiles, 13 cross-sections were excluded and not considered in the thermal simulations. The average temperature on the steel profile flanges should be determined by:

$$\theta_{f,t} = \theta_{0,t} + k_{IM,t}(u/A)_p + k_{f,t}(t_f) \quad [^\circ C] \tag{1}$$

where the sub-index t represents the fire rating in minutes, $\theta_{f,t}$ is the average temperature of the flanges, expressed in degrees Celsius [°C], $\theta_{0,t}$. is a reference value expressed in degrees Celsius [°C], according to Table 4. The parameter $(u/A)_p$. is the section factor of the PEC. The parameters $k_{IM,t}$ and $k_{f,t}$ are empirical coefficients that are directly related to the section factor and the thickness of the flange (t_f) for each required time of fire resistance, respectively. The parameters and coefficients are defined according to Table 4.

Lear regression was used to calculate the best polynomial that fits the numerical rults. The regression model's coefficient of determination (R^2) to estimate the average flange temperature was 0.98 for R30, 0.97 for R60, 0.96 for R90, and 0.94 for R120. From Eq. 1, one can determine the factors $k_{y,\theta}$ and $k_{E,\theta}$, to reduce the mechanical properties of steel flange components (yield stress and the modulus of elasticity).

The plastic resistance to axial compression and the effective flexural stiffness of the flanges can be determined from Eq. (2) and Eq. (3).

$$N_{fi,pl,Rd,f} = \frac{2 \cdot \left(b_c \cdot t_f \cdot f_{ay,\theta,f}\right)}{\gamma_{M,fi,a}} \quad [N] \tag{2}$$

$$(EI)_{fi,eff,z,f} = \frac{E_{a,\theta,f} \cdot t_f \cdot b_c^3}{6} \quad \left[N.mm^2\right] \tag{3}$$

Table 3 Materials and general mechanical properties

Standard	Material	Denomination	Parameters	Values
American steel section	Structural profile steel	ASTM A572 Gr.50	E_a[GPa]	200
			f_{ay}[MPa]	345
	Concrete	C20	f_{ck}[MPa]	20
			E_{cm}[GPa]	30
	Reinforcement steel	CA-50	E_s[GPa]	200
			f_{sy}[MPa]	500
European steel sections	Structural profile steel	S275	E_a[GPa]	210
			f_{ay}[MPa]	275
	Concrete	C20	f_{ck}[MPa]	20
			E_{cm}[GPa]	30
	Reinforcement steel	S500 NR Class B	E_s[GPa]	210
			f_{sy}[MPa]	500

3.2 Web of the Steel Profile

The new proposal differs from the simple calculation method in Annex G.3 of [4] where only a residual web area is considered. The new proposal considers the entire area of the web to determine the resistance of this component.The mechanical properties of the web will be affected by the elevated temperature of this component, using a similar procedure that has been used for the flange. This proposal is only valid for PEC section factor greater than 9.0 [m^{-1}] and with a flange thickness smaller than 30 [mm]. Parameters were also established considering the size ratio between the height and width (d_c/b_c). The average temperature in the steel profile web must be determined using Eq. (4).

Table 4 Parameters for the flange temperature

Standard fire resistance	$\theta_{0,t}$ [°C]	$k_{IM,t}$ [m.°C]	$k_{f,t}$ [°C/mm]
R30	730	1.80	−5.50
R60	905	1.50	−3.30
R90	965	1.30	−1.00
R120	1015	1.15	−0.64

$$\theta_{w,t} = \theta_{0,t} + k_{IM,t} \cdot (u/A)_p + k_{w,t} \cdot \left(\frac{1}{A_w}\right) \quad [^\circ C] \tag{4}$$

where t is the standard fire rating in minutes, $\theta_{w,t}$ is the average temperature ofthe web, in Celsius [°C], $\theta_{0,t}$ is a reference value in Celsius [°C]. The parameter $(u/A)_p$ is the section factor of the PEC. The parameters $k_{IM,t}$ and $k_{w,t}$ are empirical coefficients that are directly related to the section factor and the inverse of the area of the web $\left(\frac{1}{A_w}\right)$, respectively.The parameters and coefficients for determining the average temperature on the web are defined according to Table 5.

The coefficient of determination (R^2) for this regression model was 0.99 for R30, 0.97 for R60, 0.96 for R90, and 0.96 for R120. Once the average temperature is determined, the reduction factors can be applied to the web of the steel profile. The yield stress and the modulus of elasticity of the web at elevate temperature defines the

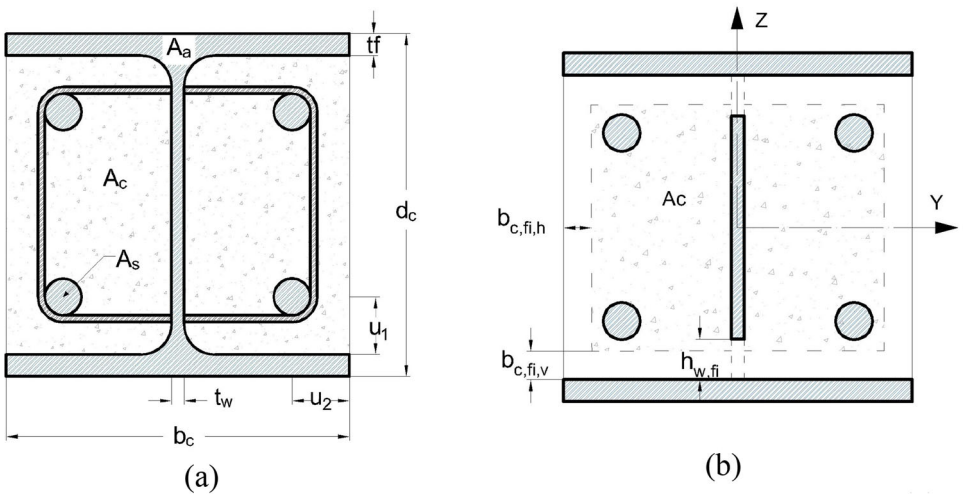

Fig. 1 Partially encased columns and the balanced summation model under fire

Table 5 Parameters for determining the average temperature in the web

Standard fire resistance	$d_c/b_c \leq 1.7$			$d_c/b_c > 1.7$		
	$\theta_{0,t}$ [°C]	$k_{IM,t}$ [m.°C]	$k_{w,t}$ [mm².°C]	$\theta_{0,t}$ [°C]	$k_{IM,t}$ [m.°C]	$k_{w,t}$ [mm².°C]
R30	−47.65	23.06	−0.05	35.51	6.92	0.24
R60	−25.59	38.25	−0.15	17.72	22.72	0.08
R90	86.59	42.09	−0.19	27.76	35.83	−0.19
R120	204.78	41.28	−0.19	84.58	40.88	−0.29

effective flexural stiffness for the weak axis and the plastic resistance to axial compression.

Unlike the current proposal G.3 of Annex G of [4], this new proposal is affecting the modulus of elasticity, keeping constant the area of the web. The plastic resistance to axial compression is also affected due to the yield stress reduction coefficient at elevated temperatures.The design of the plastic resistance to axial compression and the effective flexural stiffness of the steel web under fire shall be determined by Eq. (5) and Eq. (6).

$$N_{fi,pl,Rd,w} = f_{ay,\theta,w} \cdot \left[\frac{(d_c - 2t_f) \cdot t_w}{\gamma_{M,fi,a}}\right] \quad [N] \tag{5}$$

$$(EI)_{fi,eff,z,w} = E_{a,\theta,w} \cdot \left[\frac{(d_c - 2t_f) \cdot t_w^3}{12}\right] \quad [N.mm^2] \tag{6}$$

3.3 Concrete

The temperature field developed in the concrete core between the flanges and the core of the steel profile of the composite cross-section is based on the position of the 500 °C isothermal. This criterion has been introduced to determine the amount of concrete to be neglected for the load-bearing capacity. The nodes belonging to the temperature field with a limit of 500 °C were used to determine the average temperature of the concrete core of the PEC cross-section. It is worth mentioning that in the current version of the [4], it is possible to assume an average concrete temperature above 500 °C using the same amount of reduction of the concrete part in both principal directions, depending on the fire rating and section factor of the PEC. This last assumption is not in agreement with the temperature field observed for this component, which justifies to use the reduction in the horizontal direction (flange direction) different from the reduction in the vertical direction (web direction).

Considering that the external isothermal region of 500 °C has already significantly lost its structural strength due to the action of fire, the criterion of the isotherm of 500 °C was observed where the entire portion of concrete above this temperature was neglected. In this sense, the part of the concrete with a temperature below 500 °C was considered. The nodes belonging to the temperature field with a limit of 500 °C were used to determine the average temperature of the concrete in the cross-section. For each fire rating of R30, R60, R90, and R120, the average temperature of the remaining portion was calculated. This average temperature was used to determine the reduction coefficient of the compressive strength of the concrete.

Considering the data obtained numerically from the concrete temperature field between the flanges and the web of the PEC cross-section, Eq. (7) is presented, which estimates the average temperature inside the concrete core, considering that the load-bearing resistance of concrete has a maximum temperature of 500 °C. The new coefficients for the parameters of Eq. (7) are presented in Table 6.

$$\theta_{c,t} = \theta_{0,t} + k_{IM,t} \cdot (u/A)_p + k_{Ac,t} \cdot \left(\frac{1}{A_c}\right) \quad [^\circ C] \tag{7}$$

The value of (A_c) represents the residual area of the concrete in [m²]. If the temperature of the concrete estimated by Eq. (7) exceeds 500 °C, then it means that the entire portion of the contribution of the concrete in the calculation of the plastic resistance to axial compression and effective flexural stiffness of the concrete must be neglected. The coefficient (R^2) of the regression model used to estimate the average concrete temperature presents the value 0.99 for R30, 0.98 for R60, 0.97 for R90, and 0.97 for R120. Assuming a different reduction in both principal directions, the horizontal outer layer of concrete to be neglected is determined by Eq. (8). The coefficients of the parameters presented in the equation are shown in Table 7.The concrete area (A_c) value should be in [m²].

$$b_{c,fi,h} = b_{0,t} + k_{IM,t} \cdot (u/A)_p^2 + k_{Ac,t} \cdot \left(\frac{1}{A_c}\right) \quad [mm] \tag{8}$$

The coefficient (R^2) of the regression model used to estimate the concrete reduction presents a value of 0.25 for R30, 0.74 for R60, 0.89 for R90, and 0.86 for R120.

The reduction of vertical outer layer to be neglected should be calculated using Eq. (9). The coefficients

Table 6 Coefficients for estimating the average temperature of the concrete core

Standard fire resistance	$\theta_{0,t}$ [°C]	$k_{IM,t}$ [m.°C]	$k_{Ac,t}$ [m^2.°C]
R30	27	13.00	0.45
R60	55	16.80	2.75
R90	105	16.00	6.75
R120	125	15.80	11.00

Table 7 Coefficients for reducing the horizontal thickness of the concrete core

Standard fire resistance	$b_{0,t}$ [mm]	$k_{IM,t}$ [$mm.m^2$]	$k_{Ac,t}$ [$mm.m^2$]
R30	10.7	0.0025	0.025
R60	17.5	0.0055	0.450
R90	18.0	0.0355	1.150
R120	14.0	0.1311	1.950

presented in the equation are determined according to the application limits, and values are shown in Table 8.

$$b_{c,fi,v} = b_{0,t} + k_{IM,t} \cdot (u/A)_p^2 + k_{bc,t} \cdot \left(\frac{1}{b_c}\right) + k_{f,t} \cdot \left(\frac{1}{t_f}\right) \quad [mm] \tag{9}$$

The value of the width of the profile b_c and the thickness of the flange t_f should be in [m], see Fig. 1. There is also a differentiation in the application limit between the first and second set of coefficients to estimate the value of the vertical thickness of concrete, depending on the ratio between the height and width of the cross-section.

The coefficient (R^2) of the regression model to estimate the polynomial curve that fits the numerical data tothe vertical thickness of the concrete has a value of 0.93 for R30, 0.92 for R60, 0.95 for R90, and 0.97 for R120.

Once the horizontal and vertical reduction distances are determined, the average temperature of the concrete may be calculated based on the total number of nodes included in this region. It is worth mentioning that the mesh is regular and small (see Fig. 2) to accurately determine the position of the 500 °C isothermal. Using the results of the average temperature of the concrete and the residual area of concrete, the factor $k_{c,\theta}$ was determined to reduce the mechanical properties of concrete at elevated temperatures. The characteristic value of the compressive strength of concrete in fire conditions $f_{ck,\theta}$ directly interferes with the plastic resistance to axial compression and the effective flexural stiffness of the concrete. The design of the plastic resistance to axial compression and the effective flexural stiffness of the concrete in the fire situation should be determined according to Eq. (10) and Eq. (11).

$$N_{fi,pl,Rd,c} = \frac{0.86 \cdot \left\{\left[\left(d_c - 2t_f - 2b_{c,fi,v}\right) \cdot \left(b_c - t_w - 2b_{c,fi,h}\right)\right] - A_{s,\theta}\right\} \cdot f_{ck,\theta}}{\gamma_{M,fi,c}} \quad [N] \tag{10}$$

$$(EI)_{fi,eff,z,c} = E_{c,\sec,\theta} \cdot \left\{\left[\frac{\left(d_c - 2t_f - 2b_{c,fi,v}\right) \cdot \left(\left(b_c - 2b_{c,fi,h}\right)^3 - t_w^3\right)}{12}\right] - I_{s,\theta}\right\} \quad [N.mm^2] \tag{11}$$

Considerations regarding the area and the second moment of area of the longitudinal steel reinforcement in the fire situation are presented in the section referring to the temperature of the reinforcing bars.

3.4 Reinforcing Bars

The Annex G of [4], considers the reduction factor for the elastic modulus $k_{E,t}$ and yield stress$k_{y,t}$, depending only on the position of the reinforcing bars in the cross-section. The new proposal considers the average temperature $\theta_{s,t}$ and position of the reinforcing barsu_s, the thickness of the flange t_f,and the diameter of the reinforcing bars ϕ. The average temperature of the cross-section of the reinforcing bars has an application limit regarding the parameters

Table 8 Coefficients and parameters for reducing the vertical thickness of concrete core

Standard Fire Resistance	$d_c/b_c \leq 2.0$				$d_c/b_c > 2.0$			
	$b_{0,t}$ [mm]	$k_{IM,t}$ [$mm.m^2$]	$k_{bc,t}$ [mm.m]	$k_{f,t}$ [mm.m]	$b_{0,t}$ [mm]	$k_{IM,t}$ [$mm.m^2$]	$k_{bc,t}$ [mm.m]	$k_{f,t}$ [mm.m]
R30	−1.35	0.005	0.40	0.08	0.31	0.015	0.45	0.03
R60	8.15	0.035	2.15	0.05	18.55	0.235	−6.85	0.02
R90	−25.25	0.195	13.15	−0.11	−20.95	0.255	12.65	−0.09
R120	−54.55	0.435	22.85	−0.21	93.55	1.950	−53.65	−0.91

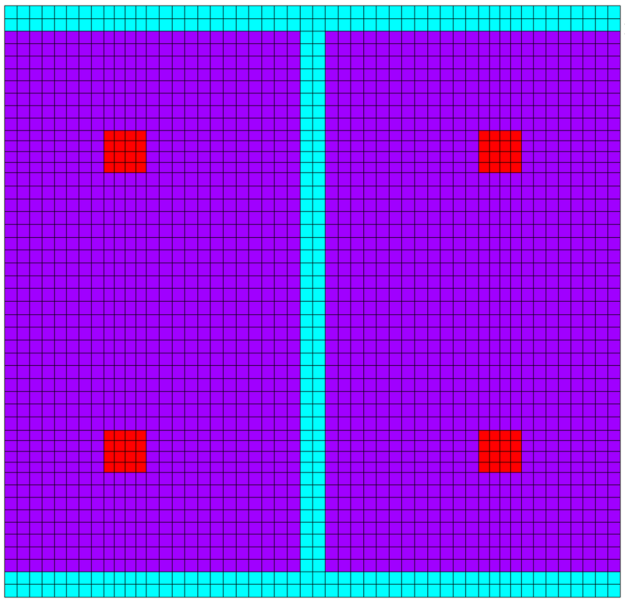

Fig. 2 Mesh size used for the analysis of the cross-section

included in Eq. (12). The application limit of this design step stands for standard fire [5]. The section factor should be higher than 9.0 [m^{-1}], and the thickness of the flanges should be smaller than 30 [mm]. The average temperature in the reinforcing bars should be determined by Eq. (12).

$$\theta_{s,t} = \theta_{0,t} + k_{IM,t}(u/A)_p + k_{s,t}(u_s) \quad [^\circ C] \tag{12}$$

where t is the fire rating time in minutes, $\theta_{s,t}$ is the mean temperature of the reinforcing bars in [°C], $\theta_{0,t}$ is a reference temperature in [° C], following the values presented in Table 9. The parameters $k_{IM,t}$ and $k_{s,t}$ are empirical coefficients that are directly related to the section factor and the parameter u_s.This new value u_s is determined by Eq. (13). The numerical simulations showed a strong correlation between the increase in the average temperature of the reinforcing bars with some geometric parameters of the PEC section, such as the horizontal and vertical axial distance vu_1 and u_2, the thickness of the flange t_f and the diameter of the reinforcement used ϕ in [mm].

$$u_s = \sqrt{(u_1 + t_f)^2 + u_2^2 + \phi^2} \quad [mm] \tag{13}$$

The parameters and coefficients used to estimate the average temperature of the reinforcing bars are defined in Table 9.

The parameters used in Eq. (12) depend on the ratio between the height and width of the cross-section of the PEC and the section factor. The coefficient (R^2) of the regression model to estimate the average temperature of the reinforcing bars presented the value 0.94 for R30, 0.98 for R60, 0.98 for R90, and 0.97 for R120. The reduction factors $k_{ys,\theta}$ and $k_{Es,\theta}$ were determined for the average temperature of the reinforcing bars. The contribution of this component to the effective flexural stiffness and the plastic resistance to axial compression is given by Eq. (14) and (15).

$$N_{fi,pl,Rd,s} = \frac{A_{s,\theta} \cdot f_{sy,\theta}}{\gamma_{M,fi,s}} \quad [N] \tag{14}$$

$$(EI)_{fi,eff,z,s} = E_{s,\theta} \cdot I_{s,\theta} \quad [N.mm^2] \tag{15}$$

Table 10 compares the current version of the balance summation of the [4] and the new proposal, considering the same four components.

4 Advanced Calculation Method

The calculation of the temperature field in the cross-section of PEC was obtained by the Finite Element Method, using ANSYS software, based on the 2D analysis of the cross-section and 3D analysis of the entire PEC column.

The temperature depends on the space and time,$T = T(x, y, z, t)$ and the solution is non-linear by the effect of the temperature dependence and boundary conditions. The emissivity for steel and concrete has been defined at 0.7, the thermal conductivity of the concrete has been considered with the upper limit, and the concrete's moisture established at 3%. The boundary conditions for the 2D and 3D thermal models are applied following the recommendations of the [32]. On the exposed surface, radiation applies, using the ε_f = 1 and the gas temperature from [5]. The convection condition should also be applied using the convection coefficient α_c = 25 [W/m^2.K]. The initial condition was defined in 20°C applied to all nodes. Material properties were determined according to the Eurocodes dedicated for each material. [33] already carried out the validation of the numerical model.

The nonlinear thermal analysis is solved with an integration time step of 60 s, with the possibility of reducing to 1 s. The convergence criterion uses a heat flow tolerance

Table 9 Parameters for determining the average temperature in the reinforcing bars

Standard fire resistance	$d_c/b_c \le 1.7$ $(u/A)_p \le 20.0$			$d_c/b_c > 1.7$ $(u/A)_p > 20$		
	$\theta_{0,t}$ [°C]	$k_{IM,t}$ [m.°C]	$k_{s,t}$ [°C/mm]	$\theta_{0,t}$ [°C]	$k_{IM,t}$ [m.°C]	$k_{s,t}$ [°C/mm]
R30	290	1.05	−1.20	220	8.85	−1.35
R60	435	8.65	−1.65	505	11.50	−2.45
R90	535	12.90	−1.75	690	10.85	−2.75
R120	675	12.50	−1.95	725	12.65	−2.35

Table 10 Comparison between [4] and the new proposal

Element	[4]	New proposal
Flange	Area: Not reduced; Temperature: Linear trend: $\theta_{f,t} = \theta_{0,t} + k_t(u/A)_p$ E_a: (affected by temperature); f_{ay}: (affected by temperature)	Area: Not reduced; Temperature: New proposal: $\theta_{f,t} = \theta_{0,t} + k_{IM,t}(u/A)_p + k_{f,t}(t_f)$ E_a (affected by temperature); f_{ay} (affected by temperature)
Web	Area: Reduced based on empirical equation (fire resistance class and geometry); $h_{w,fi} = 0.5(d_c - 2t_f)\left[1 - \sqrt{1 - 0.16\ (H_t/d_c)}\right]$. Temperature: Not calculated; E_a: (not affected); f_{ay}: (affected by temperature)	Area: Not reduced; Temperature: New proposal: $\theta_{w,t} = \theta_{0,t} + k_{IM,t} \cdot (u/A)_p + k_{w,t} \cdot \left(\frac{1}{A_w}\right)$ E_a: (affected by temperature); f_{ay}: (affected by temperature)
Concrete	Area: reduced with equal reductions in the two main directions; Temperature: Table; E_{cm}: (affected by temperature); f_{ck}: (affected by temperature)	Area: Reduced with different reductions in the two main directions; Temperature: New Proposal: $\theta_{c,t} = \theta_{0,t} + k_{IM,t} \cdot (u/A)_p + k_{Ac,t} \cdot \left(\frac{1}{A_c}\right)$ E_{cm}: (affected by temperature); f_{ck}: (affected by temperature)
Reinforcing bars	Area: Not reduced; Temperature: (by inverse method); E_s: (affected by temperature); f_{sy}: (affected by temperature); Geometrical position rebars: $u_s = \sqrt{u_1 \cdot u_2}$	Area: Not reduced Temperature: New proposal: $\theta_{s,t} = \theta_{0,t} + k_{IM,t} \cdot (u/A)_p + k_{s,t} \cdot (u_s)$ E_s: (affected by temperature); f_{sy}: (affected by temperature); Geometrical position rebars: $u_s = \sqrt{(u_1 + t_f)^2 + u_2^2 + \phi^2}$

value of 0.1% with a minimum reference value of 1×10^{-6} [W].

The thermo-mechanical solution of the entire PEC column is also obtained through an incremental loading process and iterative due to non-linearities. Different boundary conditions have been applied depending on the end conditions of the PEC. The temperature field is considered steady for each fire rating time, and the load is increased up to reach the ultimate equilibrium position. The buckling resistance of each PEC was calculated by the incremental displacement and iterative solution model using Newton Raphson method. The geometric imperfection was based on the elastic buckling mode shape with updating of the nodal coordinates. This update was based on the mode shape and based on the maximum imperfection expected on the mid high of the column corresponding to L/150. Typical incremental displacement of 0.2 mm was applied, with minimum possible incremental displacement of 0.1 mm and maximum possible incremental displacement of l mm. The criterion for convergence was based on displacement with tolerance value of 5%. The nonlinear buckling analysis is a static analysis with large deflection (equilibrium deformed configuration), extended to a point where the structure reaches its ultimate limit state (plasticity, modification into a mechanism). The buckling load bearing is the maximum load determined from the reaction on the bottom of the PEC. The 3D thermomechanical model was already validated in the work of [28].

4.1 The 2D Thermal Model

The 2D model uses the PLANE55 finite element, with four nodes and one degree of freedom per node, allowing the transient nonlinear thermal analysis to be performed. The selected element uses linear interpolation functions to determine the conductivity matrix and four integration points (2×2 Gauss point).The high number of elements is justified by the need to measure the residual area of concrete. The reinforcing bars were assumed with a square geometry to ensure a regular mesh, their sides are related to the original circular area. This model considers perfect contact between the four components, see Fig. 2.

The temperature results are presented in Fig. 3, as an example, for PEC section defined by the steel profile HP 250 × 62.0. One can see the need to differentiate the residual area of concrete in both principal directions.

4.2 The 3D Thermal Model

The 3D model uses the SOLID70 finite element, which has eight nodes, each with a single degree of freedom, the nodal temperature. This element will be applied to the steel profile, concrete, and reinforcement volume material, assuming perfect contact between materials. The interpolating functions are linear and the element uses full integration points (2 × 2x2 Gauss point) to define the conductivity matrix.

4.3 The 3D Mechanical Model

The 3D model uses the SOLID185 finite element to analyze the steel profile and the reinforcing bars, while the SOLID65 finite element has been used to the concrete. The SHELL181 finite element was used to assess the rigid plates on both ends of the PEC column. These rigid plates help distribute the localized effect of the support and load. The SOLID185 finite element has eight nodes with three degrees of freedom at each node (u_x, u_y and u_z), and uses linear interpolation functions. The element has plasticity and can be used with large displacements. The full integration option with the B-bar method was used. The B-bar method helps to prevent volumetric locking in almost incompressible cases. It replaces the volumetric deformation at the Gauss integration point by the mean volumetric deformation of the elements (selectively reduced integration technique).The SOLID65 element was used to the concrete mesh. This element includes eight nodes with three degrees of freedom in each node (displacements) and uses linear interpolating functions with a complete integration scheme (2 × 2x2 Gauss point). The model does not include the option for crack and crushing detection. The thermo-mechanical modelis composed of three types of Finite Elements and four types of materials, as shown in Fig. 4. The steel profile and the reinforcing barsuse the SOLID185 finite element. The concrete core between flanges uses SOLID65. Two end plates are used in the extremities, simulating highly rigid material, as mentioned before.

Figure 5 represents the deformed shape mode of the PEC after 30 min of fire exposure. Von Mises stress is plotted to show that the material undergoes elastic and plastic deformations.

4.4 Numerical Model Validation and Convergence Test

The numerical model was validated in the analysis of PEC under a fire situation in two stages. The first step consisted of developing the numerical models in the ANSYS software with cross-sections, mechanical properties, and boundary conditions similar to numerical and experimental analyses in the literature and comparing the thermal analysis results of these works with the results of the numerical models found.

The second step consisted of using the results of [28] for the validation of the mechanical model and the ANSYS software with the same boundary conditions and mechanical properties of the materials.

The numerical thermal validation process aimed to guarantee that the temperature values obtained by the computational modelling agreed with the results obtained experimentally by other authors.

In the numerical thermal model, the boundary conditions took into account the phenomena of heat exchange between the medium and the structural element, as well as the normative coefficients that define them and the regions where they are applied.

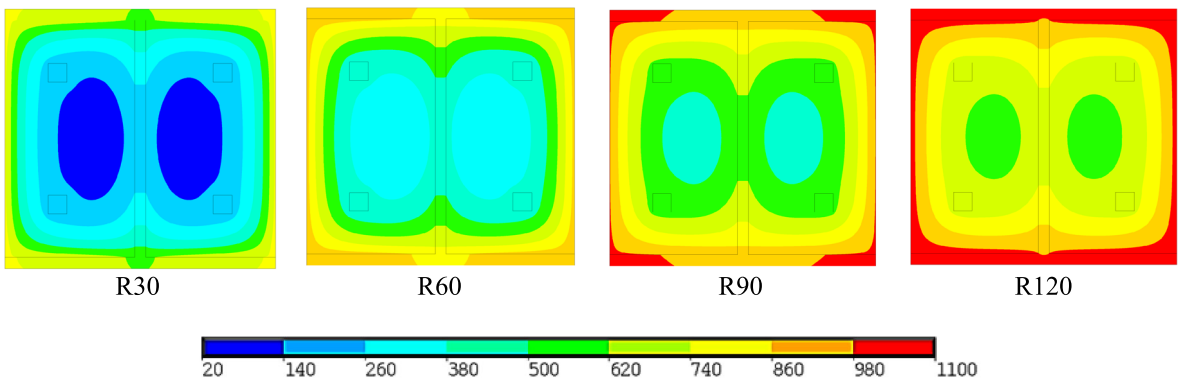

Fig. 3 Temperature results: HP 250 × 62.0 for each fire rating

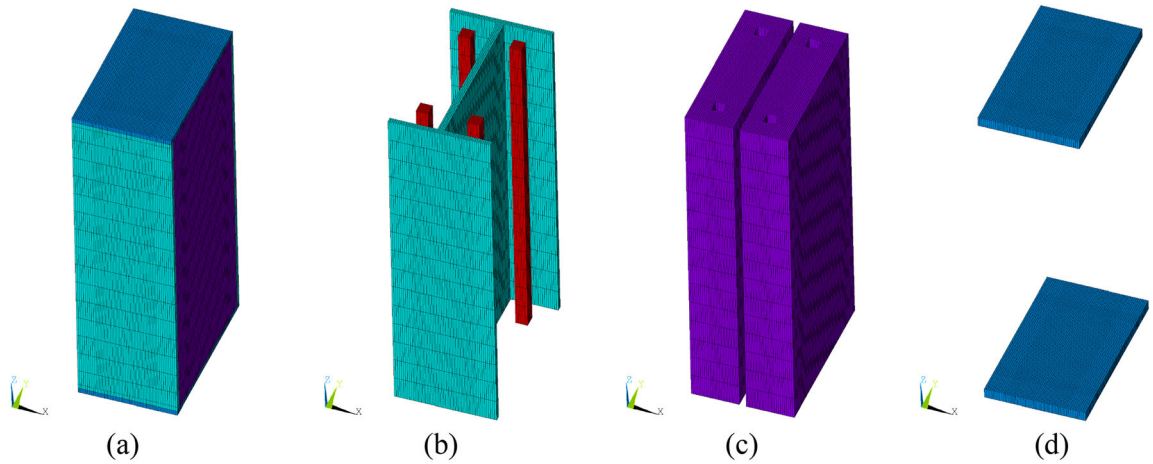

Fig. 4 Three-dimensional element meshes used in numerical simulations

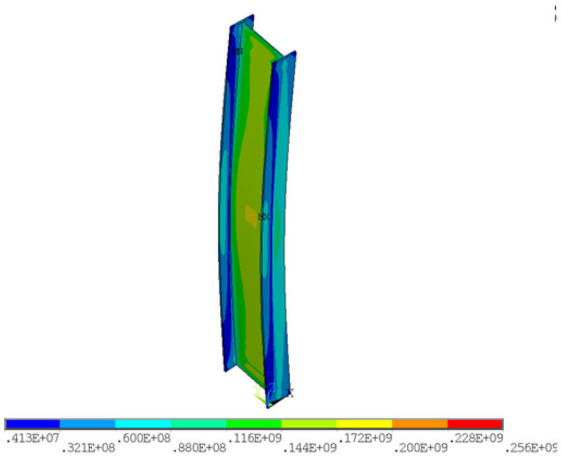

(a) Deformed shape of the steel profile

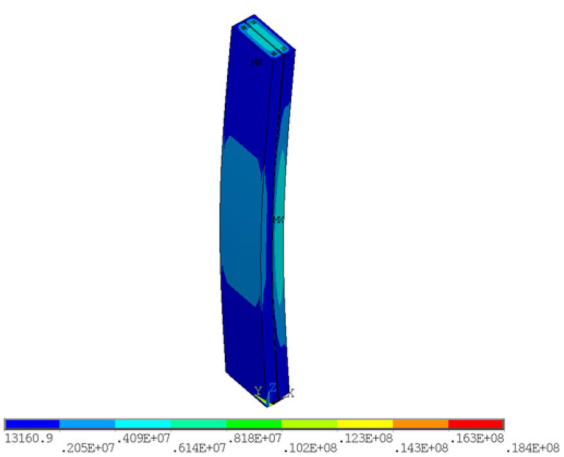

(b) Deformed shape of the concrete

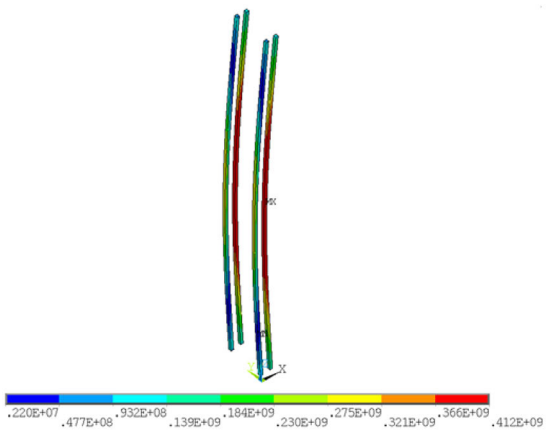

(c) Deformed shape of the reinforcing bars.

Fig. 5 Deformed shape of the PEC under fire (profile W 410 × 60), after 30 min fire exposure

Only conduction heat transfer was considered in the internal part of the structural element. The under exchanges by radiation and convection on the faces exposed under the fire were then modelled.

The numerical models were validated by comparing the variation of temperatures over time at the points considered in the experimental analyses. The comparison of the numerical models and the validation of the thermal model can be consulted in detail in [33].

These authors carried out an experimental and numerical study to evaluate how high temperatures affect the strength of the PEC. For the first cross-section, the evolution of the reinforcement bars temperature was analysed after exposure to standard fire temperatures [5] and following the criteria established by [34]. The results obtained by the authors were also compared with the results of [35]. In this validation, at a specific point on the reinforcement bar, the ANSYS numerical model reached a temperature of 388.1 °C in 90 min of fire exposure. In the work by [34], the temperature obtained was 403.0 °C, a relative difference of 3.8% between the values. In [35], the experimental model reached 389.5 °C, and its mathematical model predicted 357.9 °C at this exact point. Thus verify a relative difference between the values of this author of 0.4% and 7.8%, respectively. Therefore, in this first validation, the ANSYS numerical model obtained thermal analysis results within acceptable experimental and numerical parameters in the literature.

For the second numerical validation, [36] survey is an experimental study on lateral torsional buckling in PEC under fire. The fire of the cross-section of the numerical models showed the expected behaviour of temperature rise, using fire with a constant rate applied directly to the table nodes of the structural profile. Because of this, the need to calibrate the parameters of the computational model according to the data obtained experimentally is evident to perform numerical analyses that reflect, in the best possible way, the natural phenomena. It was found that the parameters used in the numerical model satisfactorily represented the expected temperature evolution in a full-scale test using the fire curve [5].

The experimental and numerical work by [37] was used for the third numerical validation. Later, other authors, such as [38], used this study and evaluated the structural resistance of similar construction elements when subjected to the effect of temperature rise. The relative difference in most results was less than 15% between the values obtained numerically and the experimental values from [37], thus showing significant similarity.

Regarding the mechanical model validation was first performed by of [28], which developed the 3D finite element model to validate the numerical results based on the experimental results presented by [17]. The 3D model was created with the HEA160 profile, and the material steel S355, concrete class C25/30, was used to compare the experimental and the predicted numerical results.

Comparisons between experimental temperature results and numerically predicted temperature versus time curves of the PEC column showed good agreement. A reasonably good agreement was found between the numerical predictions and the experimental results. The numerical results were slightly higher than those of [17] and the material is considered in perfect contact, which can explain higher temperatures on the numerical results, however, in the real cases contact may not be perfect.

The numerical results of the axial restraining forces over the fire exposure time were compared with [17]. The numerical results were almost similar to the experimental results, with a less than 10% difference. Therefore, the numerical results agree with those of the experimental results, and the model proved to be accurate in predicting the load-bearing capacity of PEC under fire. The validation of the mechanical model can be consulted in detail in [28].

Thus, the validation process of the numerical model ensures that the temperatures used later as results of numerical simulations to determine the thermos-structural behaviour of the PEC have good agreement with experimental results found in the literature.

Regarding the mesh convergence test of 2D and 3D models was performed with different meshes sizes due to best represents the PEC from computational limitations.

The 2D mesh of finite elements was modelled in a rectangular shape, with the finite elements of all cross-sections under study measuring 1.15 mm on each side. The longitudinal reinforcement bars were modelled with a square geometry, with approximately the same cross-sectional area, their sides equivalent to the original circular section. In addition, the model considers the perfect contact between the four components.

A large number of mesh elements is justified by the need to precisely measure the residual area of the concrete, taking into account the 500 °C isotherm, obtaining good resolution of the respective horizontal and vertical distances from the residual area to the face of the section flange transverse.

For the definition of the finite element mesh, the best computational cost–benefit was considered, considering the time taken to run the simulations, the large volume of data, and the accuracy of the results. Thus, respecting the proportionality of its dimensions, values between 1:1:3 and 1:1:20 were adopted, with the maximum proportion being 1:1:50. Therefore, results were obtained with acceptable precision in the field of temperatures and in the resistant efforts of the three-dimensional models of PEC in fire situation.

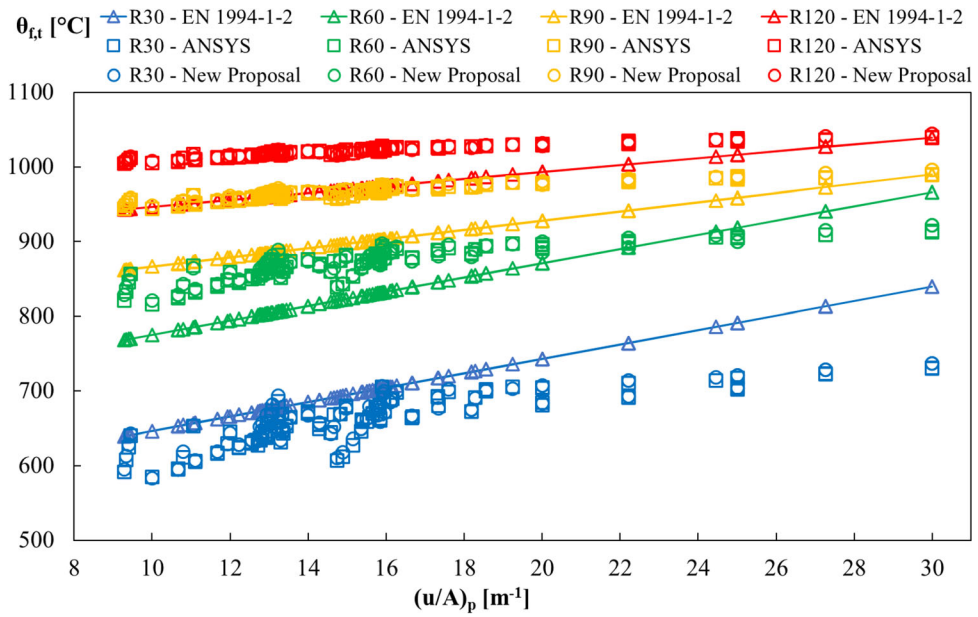

Fig. 6 Comparison of the average temperature of the flanges

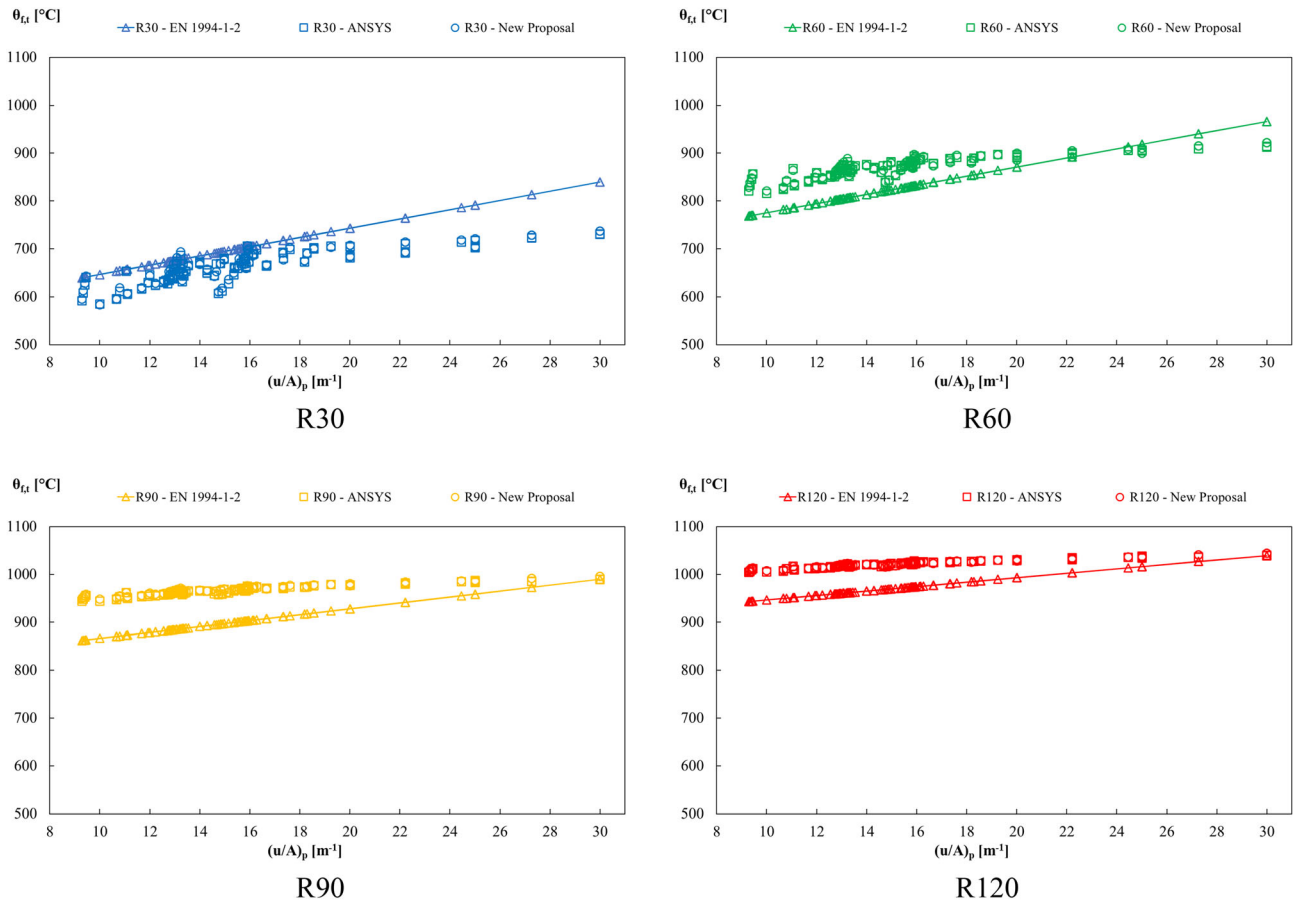

Fig. 7 Comparison of the average temperature of the flanges separately

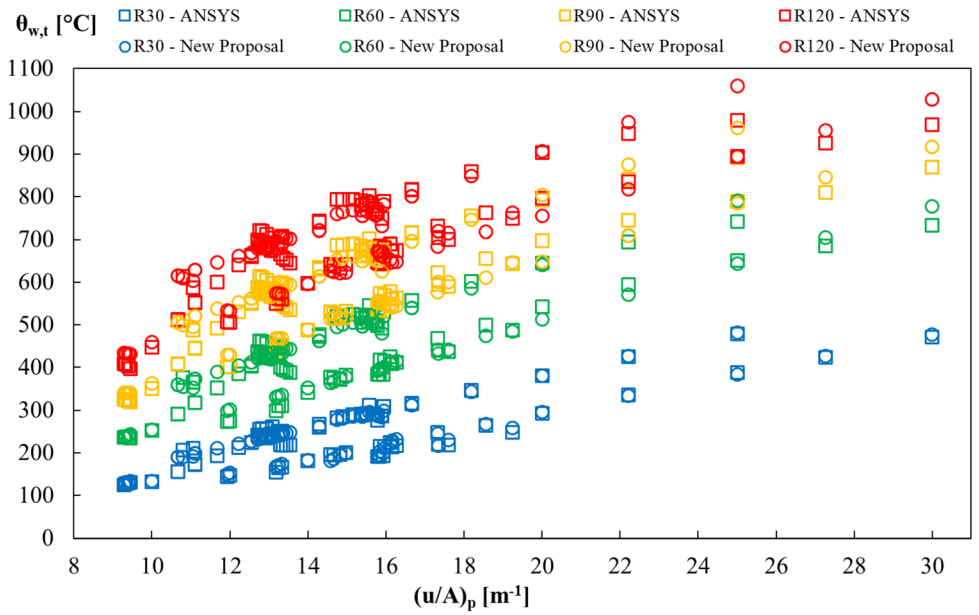

Fig. 8 Average temperature of the web of steel profiles

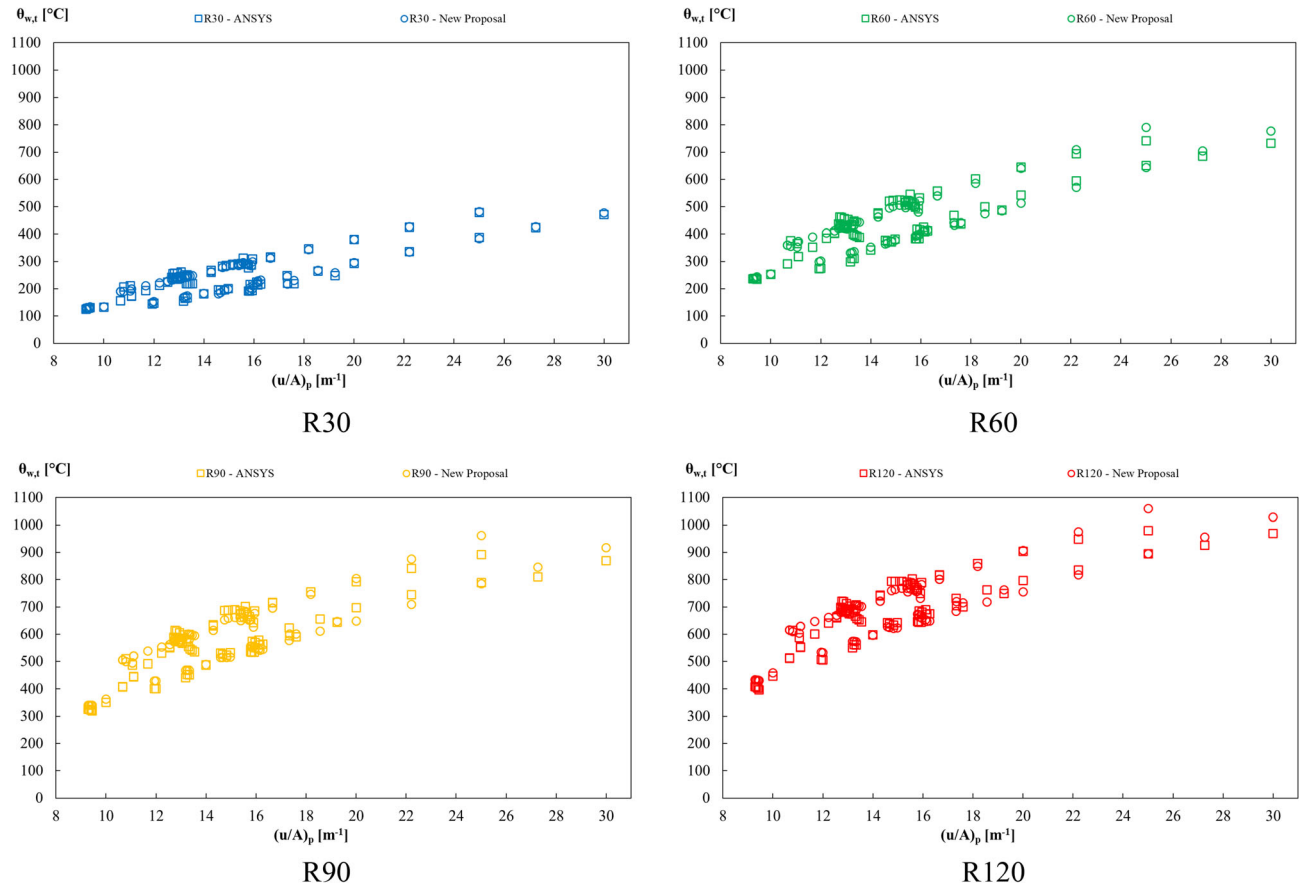

Fig. 9 Average temperature of the web of steel profiles separately

Regarding the limit for vertical displacement and geometric imperfection, to ensure the integrity of the building in a fire situation, the British standard [39] outlines the general principles for determining the resistance of structural elements when subjected to standardized fire conditions. To determine the load-bearing capacity, the standard establishes a performance criterion in which the element must maintain its support capacity during the test duration.

For elements subjected to vertical loads, the [39] establishes crushing limits and vertical contraction rate of the element subjected to axial load. The maximum deflection must also be evaluated, as well as the evolution of the deflection rate. In a simplified way, only the crushing limit was used to establish the end of the numerical simulation and obtain the resistance values to the plastification of the PEC under fire.

As for the criterion of maximum geometric imperfection for the non-linear analysis of PEC, the limit established by item 6.7.3.6 of [40] was applied for the case of bending around the weak axis.

The limit values of geometric imperfections were used to update the deformed geometry of the structural element (initial position of the nodes) and thus impose the criteria of geometric imperfections in the numerical simulations.

To obtain the axial force for calculating PEC under fire in the nonlinear numerical simulations, the physical nonlinearities of the materials, the nodal temperatures at each instant of interest, and the geometric imperfections of the structural element were considered.

The present work evaluates the numerical models in their thermal response to reformulate the determination of the average temperature in each of the components of the cross-section and the mechanical response that considers the effects of mechanical actions and geometric imperfections, in addition to thermal actions in materials where the variation of its mechanical properties change a function of temperature, to suggest the use of a new imperfection factor to adjust the buckling curve in the design of PEC cross-sections in the fire situation.

5 Numerical Results

The temperature and displacement will be presented in this section for every fire rating time. The thermal analysis was based on a 2D model to develop the new proposal for the balanced summation model. The thermal analysis based on a 3D model was developed to find the temperature of the entire element to establish the thermo-mechanical analysis. This full 3D model can determine complex deformed shape modes, with localized effects on PEC that are not detectable by any other analysis technique, such as the 3D Beam models.

5.1 Nonlinear Transient Thermal Analysis 2D and 3D

The results of the thermal analysis were obtained with ANSYS, respecting the standard fire [5] and the boundary conditions defined in [32]. The average temperature will be determined for each component and compared with the current version [4] and the new proposal.

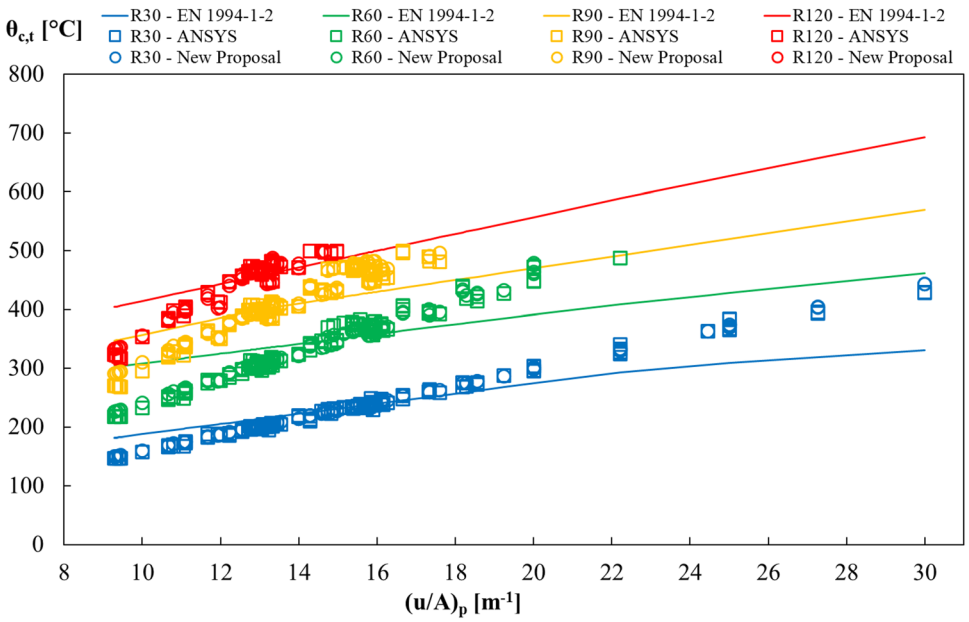

Fig. 10 Average concrete temperature

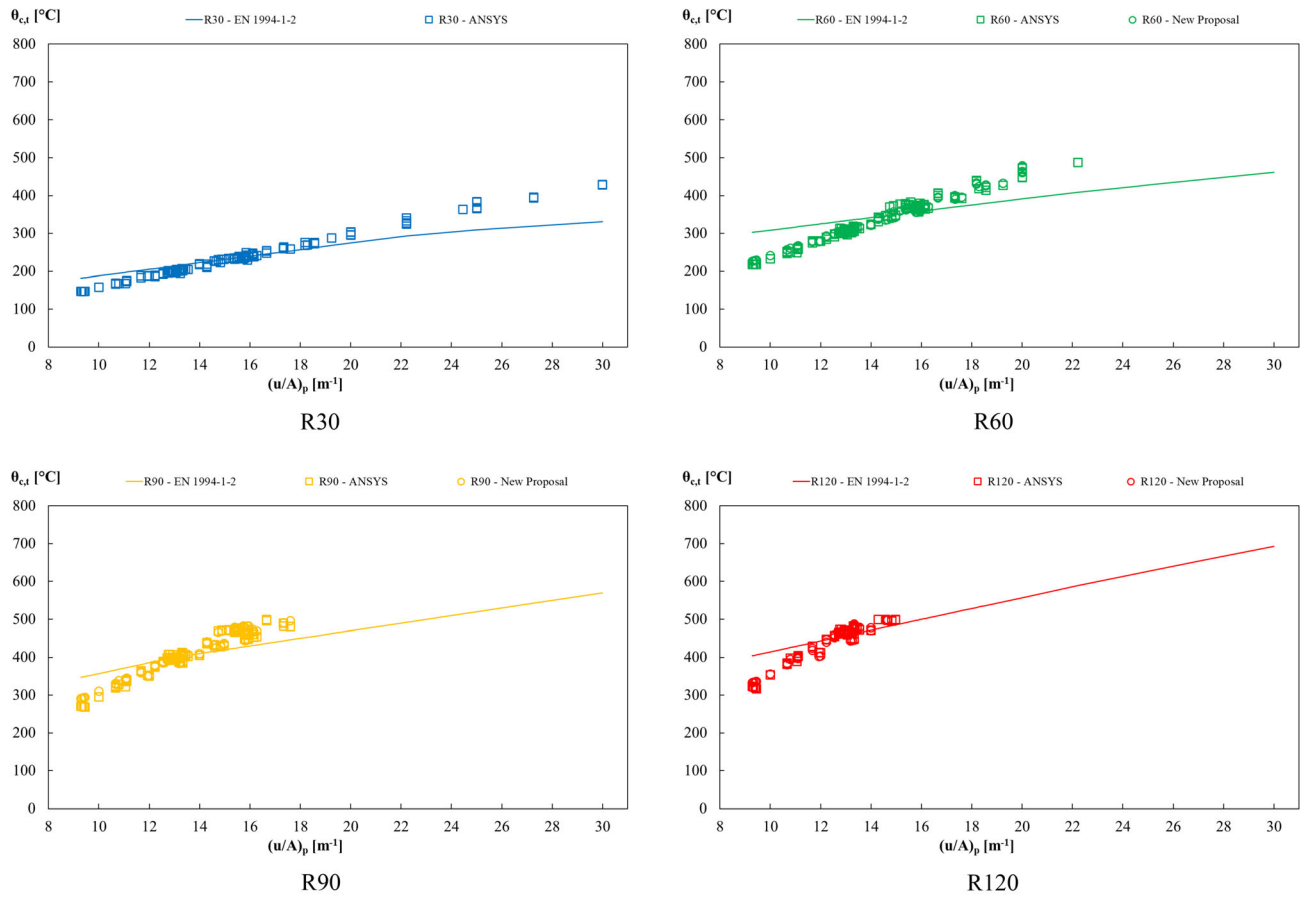

Fig. 11 Average concrete temperature separately

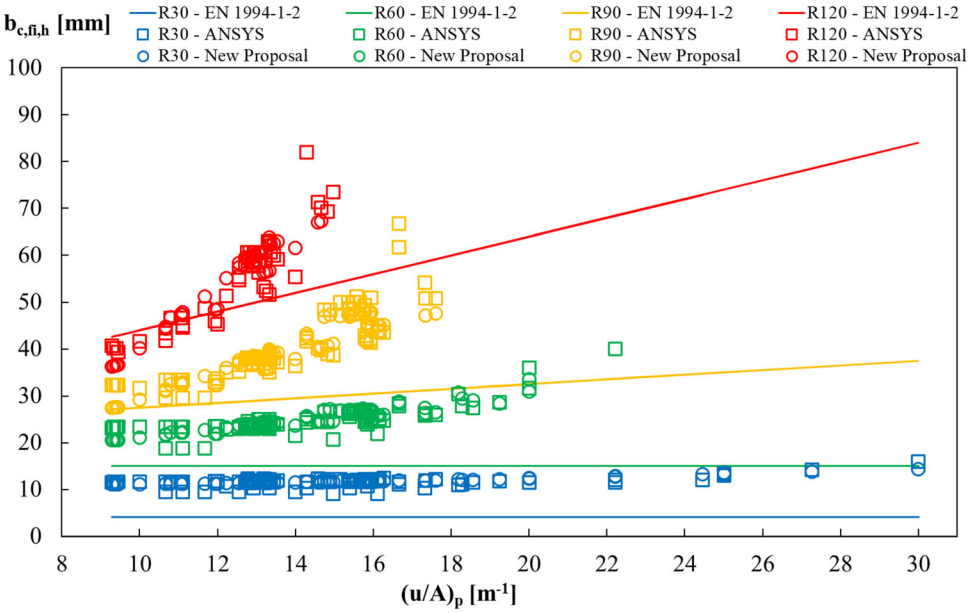

Fig. 12 Horizontal thickness reduction of the concrete area

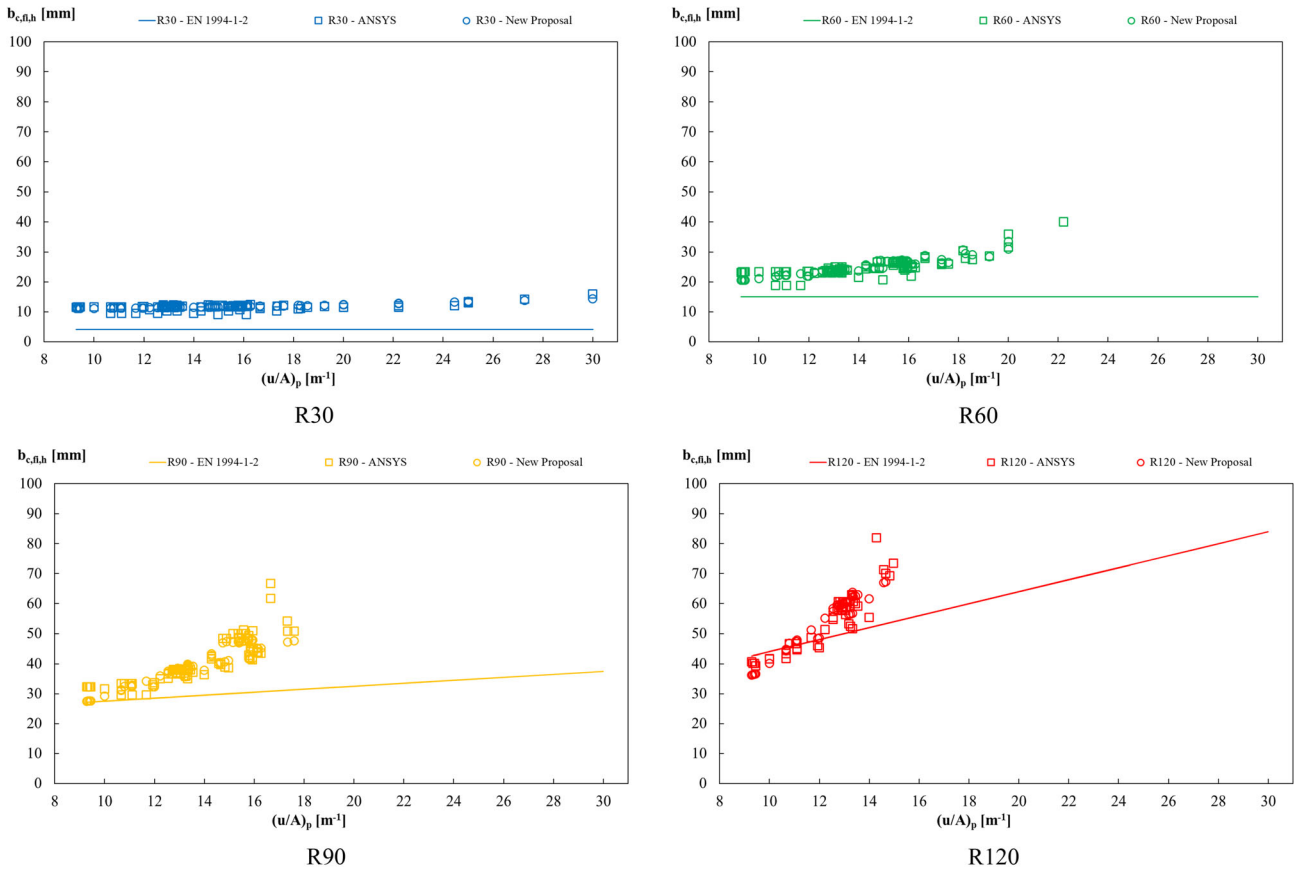

Fig. 13 Horizontal thickness reduction of the concrete area separately

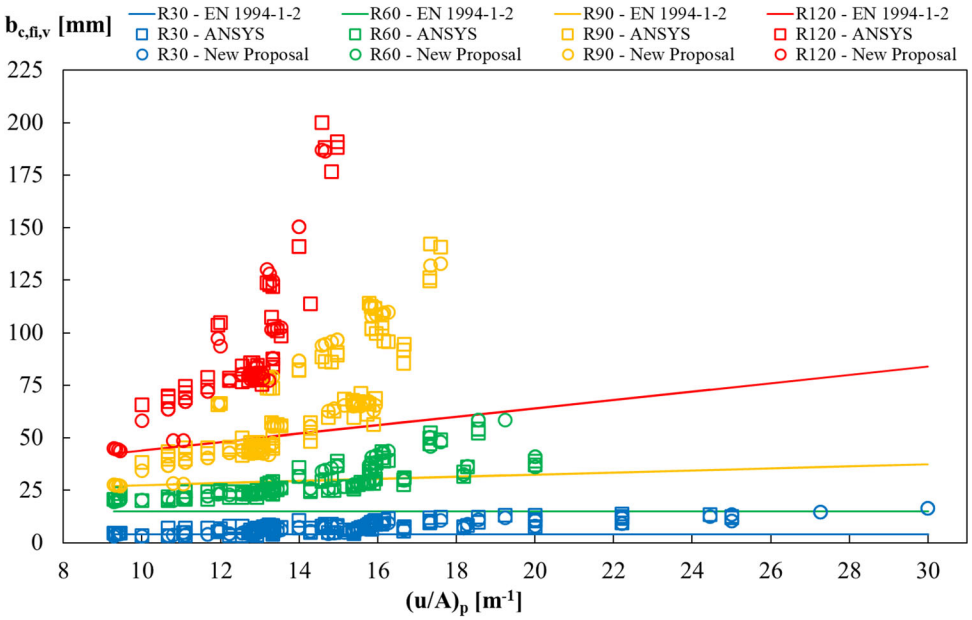

Fig. 14 Vertical thickness reduction of the concrete area

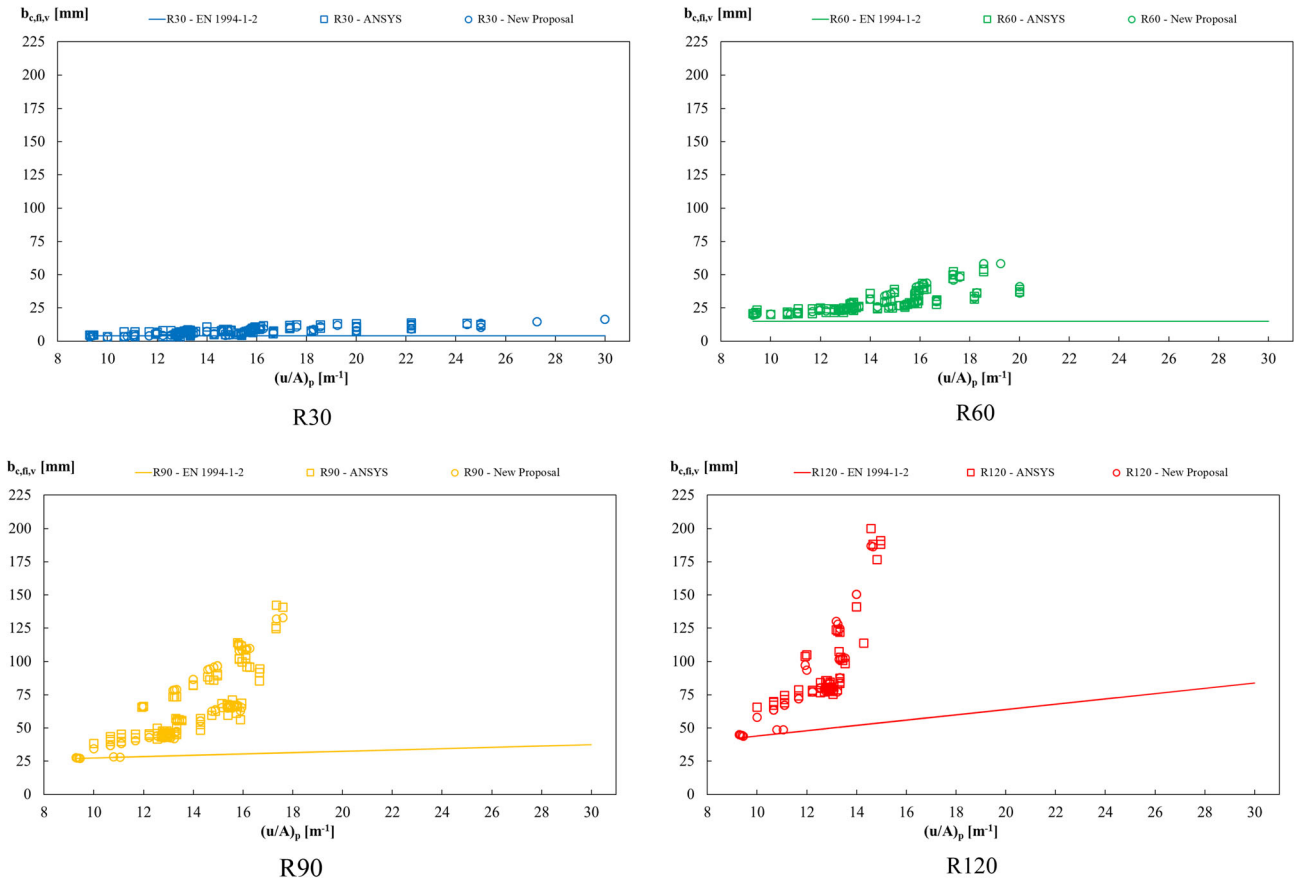

Fig. 15 Vertical thickness reduction of the concrete area separately

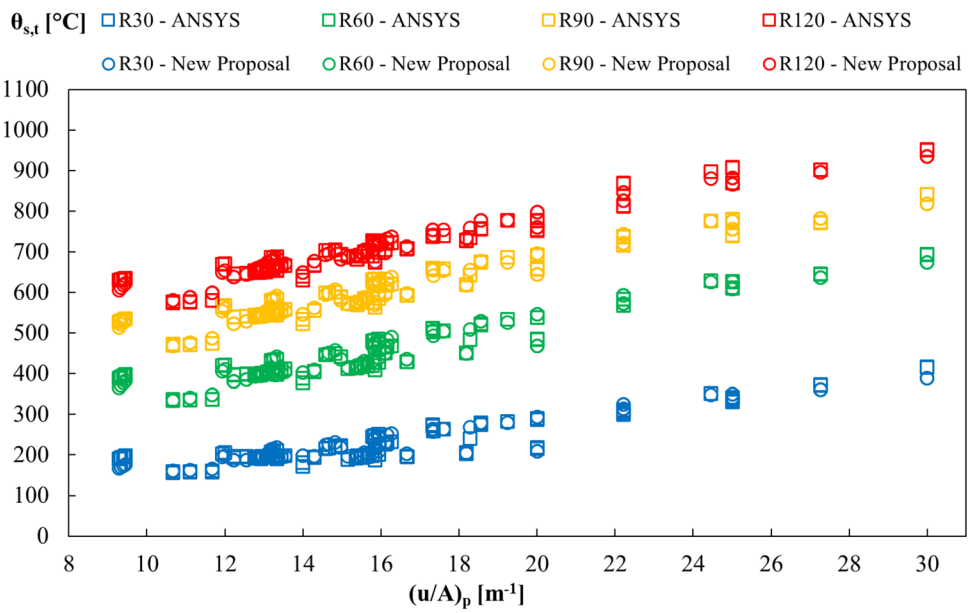

Fig. 16 Average temperature of the reinforcing bars

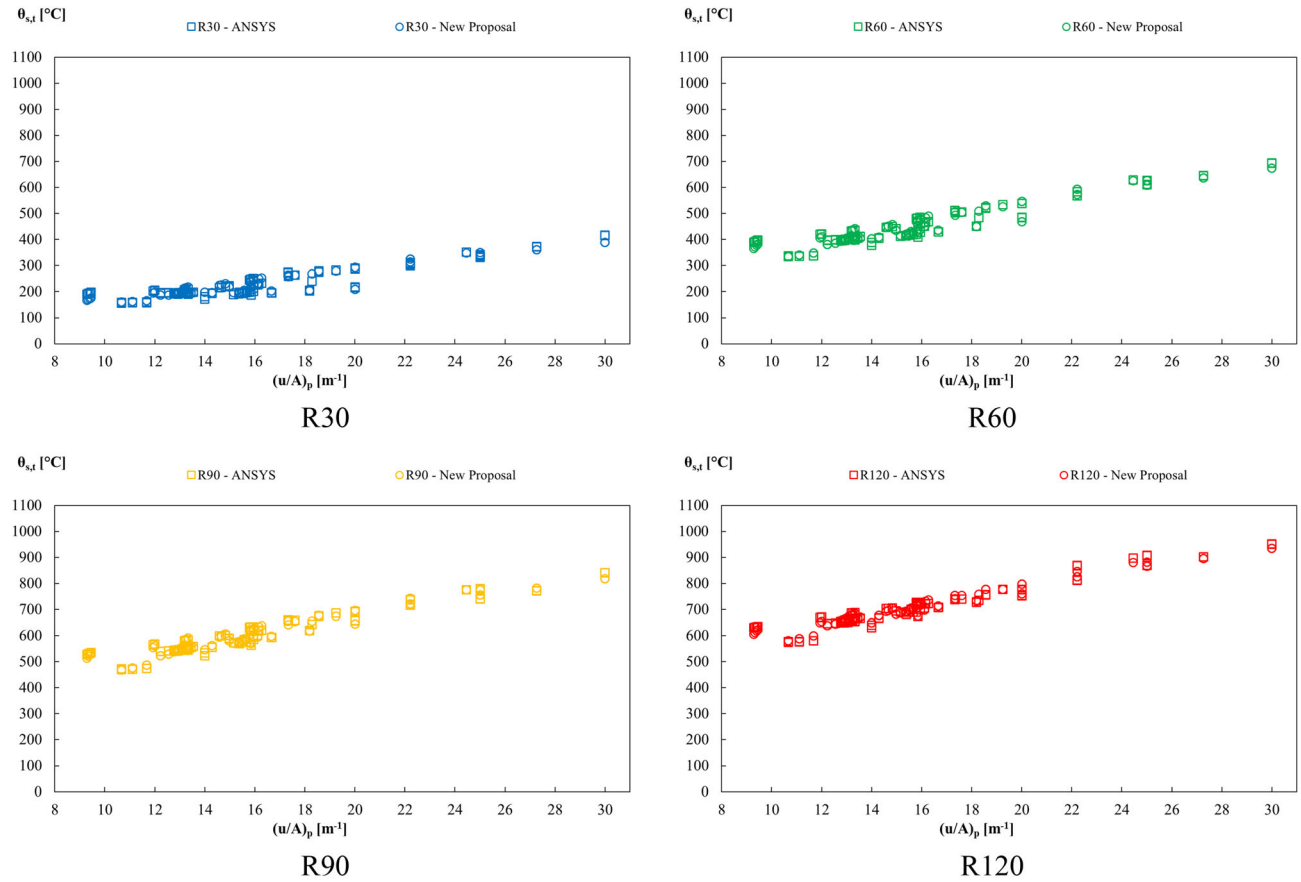

Fig. 17 Average temperature of the reinforcing bars separately

5.1.1 Temperatures of the Flanges of the Steel Srofiles

The arithmetic average of the nodal temperature of the 2D mesh provided in the flanges of the profile is determined. Figure 6 depicts the temperature of the flange depending on the section factor and fire rating. This figure compares the temperature determined by [4], with the numerical results and the new proposal. The current recommendation of [4] overestimates this temperature for the case of lower fire rates and underestimates for the possibility for higher fire rates.

Figure 7 shows the comparison of the average temperature of the flanges separately for each fire rating.

The relative difference between the numerical results and the new proposal, Eq. (1), is in the order of 1%, which reflects a good approximation. Maximum relative

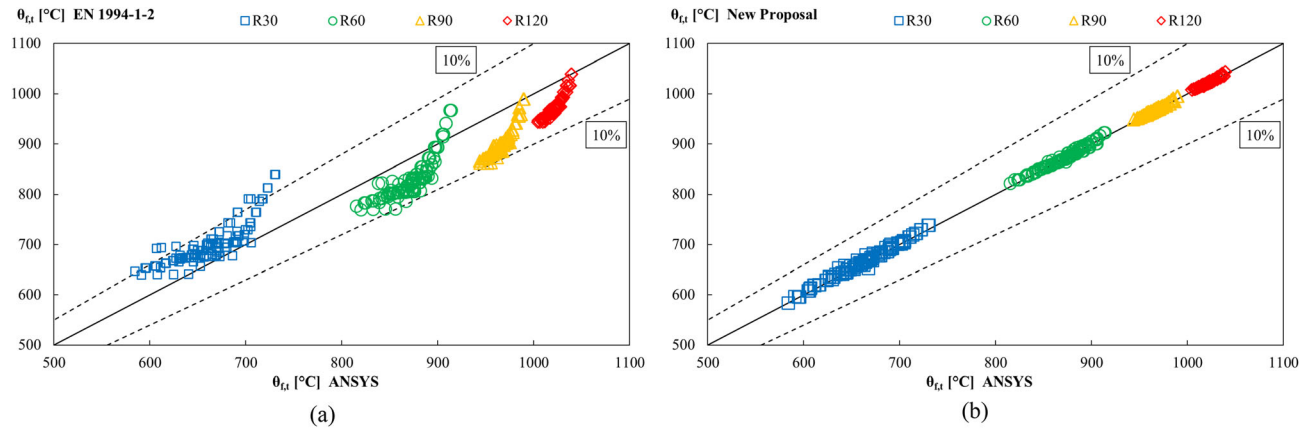

Fig. 18 Comparison of the average temperature of the flanges- (**a**) [4] (**b**) New proposal

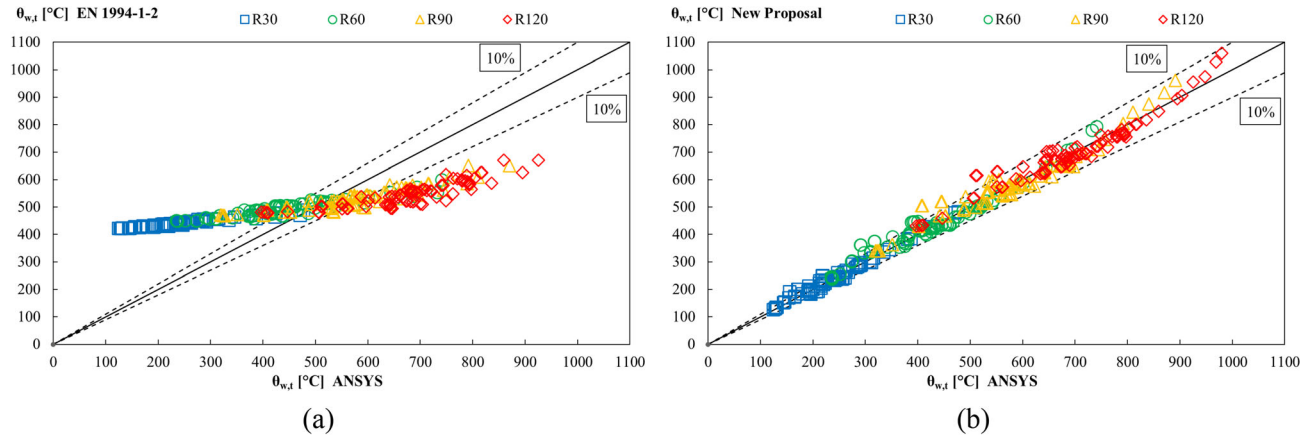

Fig. 19 Comparison of the average temperature of the web—(**a**) [4] (**b**) New proposal

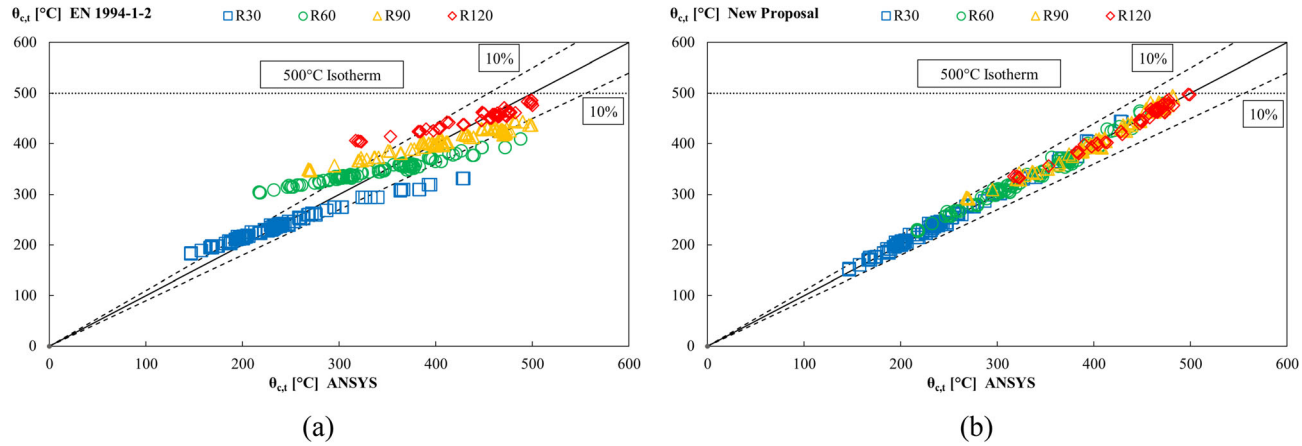

Fig. 20 Comparison of the average temperature of the concrete- (**a**) [4] (**b**) New proposal

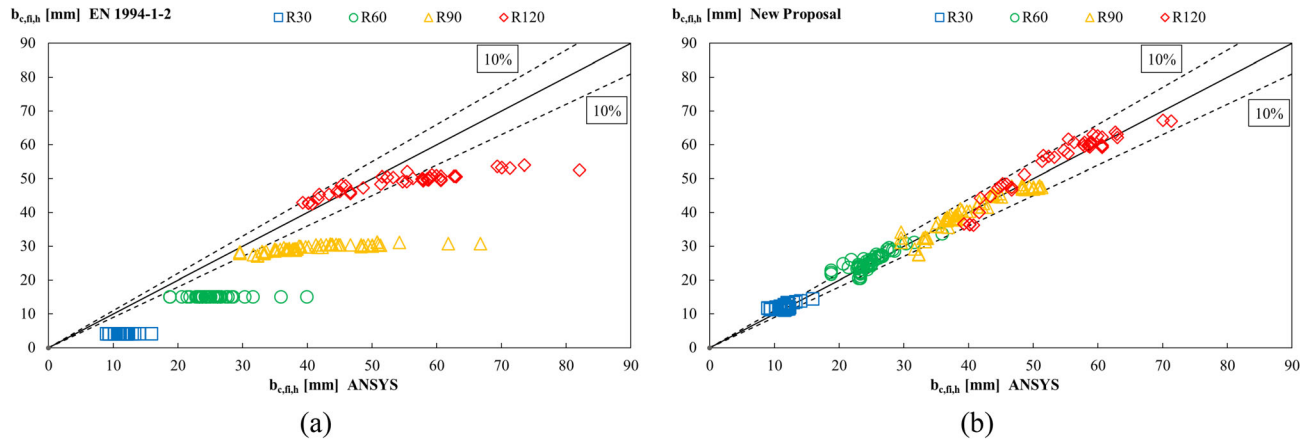

Fig. 21 Comparison between the horizontal thickness reduction of the concrete area

differences are in the order of 15%, especially in higher fire ratings and for lower section factors. The higher the temperature developed in this component, the greater the reduction in the mechanical properties of the materials, which means that the structural element will present a lower bearing capacity. So, when [4] admits lower temperature values than those being determined in the cross-section, the current standard seems to be unsafe.

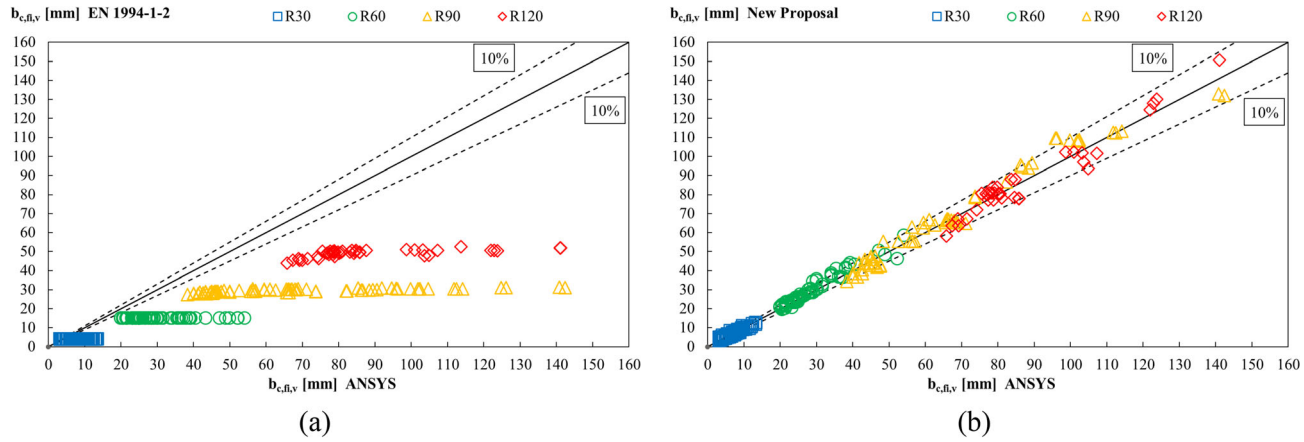

Fig. 22 Comparison between the vertical thickness reduction of the concrete area

5.1.2 Temperatures of the web of the steel profiles

This temperature was estimated using the average of the nodal temperatures. Figure 8 depicts the effect of the section factor and the fire rating when considering the original web area (without reduction). [4] does not present any simple calculation method for the temperature of this component.

Figure 9 shows the comparison of the average temperature of the web of steel profiles for each fire rating.

The average temperature determined by Eq. (2) presents a good agreement with the numerical results. The most significant differences are determined for R90 and R120 minutes and section factors higher than 22.

5.1.3 Concrete: Average temperature and residual section

The average temperature of the concrete core of the PEC cross-section was determined by the average nodal temperature included in the residual area.The location of the 500°C isotherm defined the residual area. The modified 500 °C isotherm method has been adapted to PEC sections to determine the heat-damaged zone, which comprises a general reduction of the cross-section size. Therefore, the 500 °C isotherm criterion was used, and the entire portion of concrete above this temperature was neglected. The nodes belonging to the temperature field with a limit of 500 °C were used to determine the average temperature of the concrete core of the PEC cross-section. This criterion should not be confused with the 500 °C isotherm method, initially developed by [8] and included in [30]. In this case, the temperature of the residual area is not considered at room temperature. It is also worth mentioning that in [4], it is assumed the average concrete temperature above 500 °C, depending on the fire rating and section factor of the PEC. The average temperature of the new proposal may be determined by Eq. (7). Figure 10 presents the average temperature of the concrete, depending on the section factor and fire rating. There is a good agreement between the new proposal and the numerical results. [4] overestimates the concrete temperature for lower section factors and underestimates for higher section factors.

Figure 11shows the comparison of the average concrete temperature for each fire ratings.

The new proposal presents different approximations for the affected zones of the concrete in the main principal directions, $b_{c,fi,h}$.perpendicular to the web and $b_{c,fi,v}$ in the parallel direction to the web. This decision is based on the temperature field determined for the cross-sections. These results are presented for the position of the 500 °C isotherm for each fire rating time. Figure 12 shows the reduction layer of concrete to be neglected for the load bearing in the direction perpendicular to the web, depending on the section factor and fire rating. The results show a good approximation between the new proposal and the numerical results. Most of the results, except for R120, are above the prescribed values in [4], showing that with this criterion (new proposal), the residual area is smaller than the proposed reduction of the [4], reducing the load-bearing capacity of the PEC.

Figure 13 shows the comparison of the horizontal thickness reduction of the concrete area for each fire rating.

Figure 14 shows the reduction layer of concrete to be neglected in the direction parallel to the web $b_{c,fi,v}$. All the results obtained by the new proposal recommend a higher reduction in the concrete affected by temperature.

Figure 15 shows the comparison of the vertical thickness reduction of the concrete area for each fire rating.

According to the results, this new proposal is leading to a higher reduction of the affected zone, suggesting a decrease in the load-bearing capacity of this component.

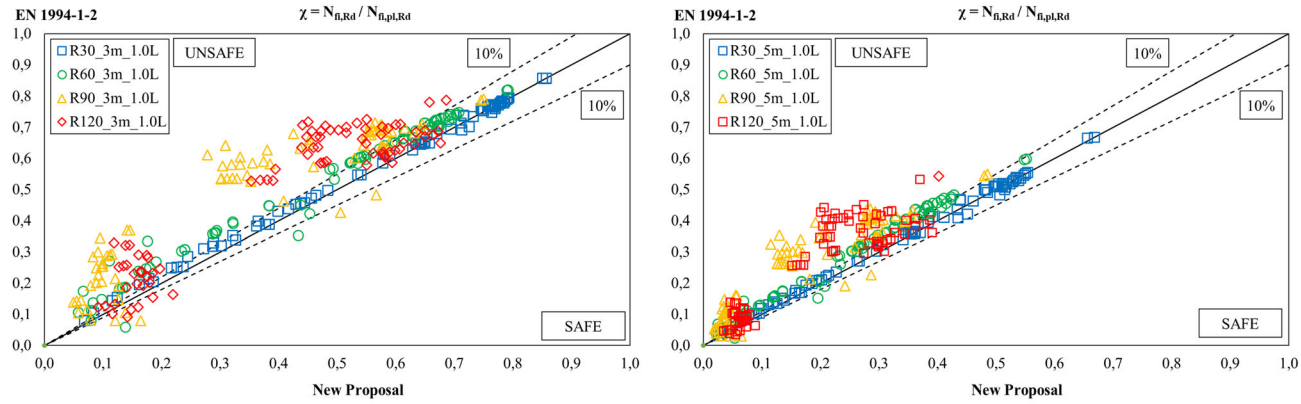

(a) Columns with 3m and 1.0L

(b) Columns with 5m and 1.0L

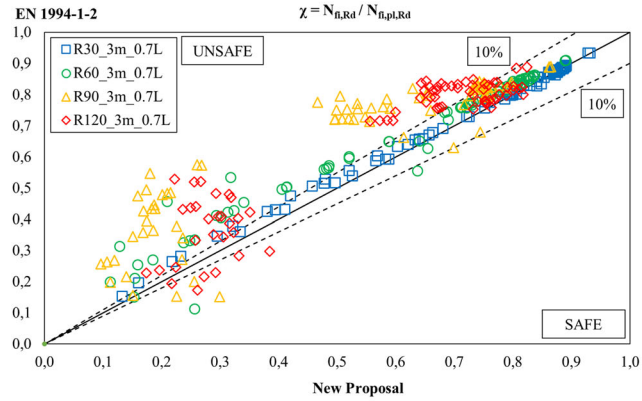

(c) Columns with 3m and 0.7L

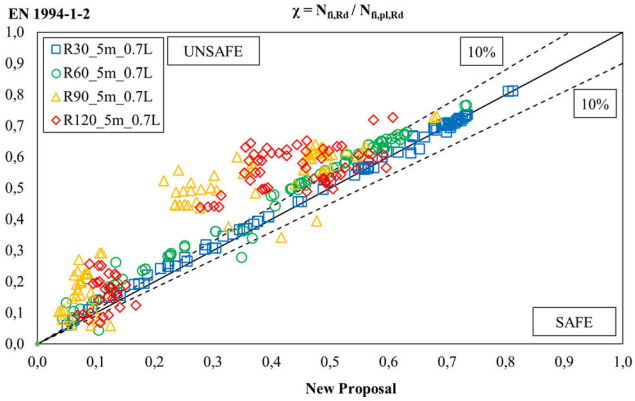

(d) Columns with 5m and 0.7L

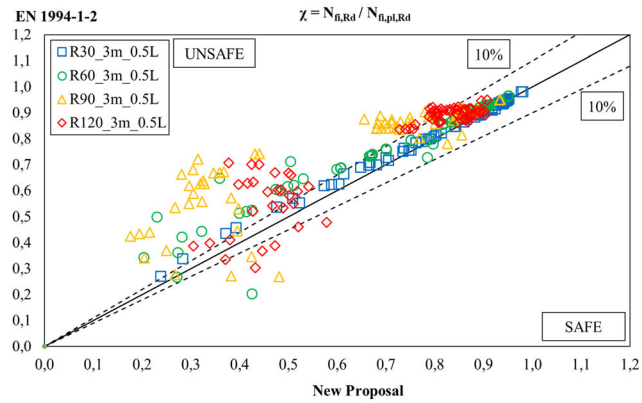

(e) Columns with 3m and 0.5L

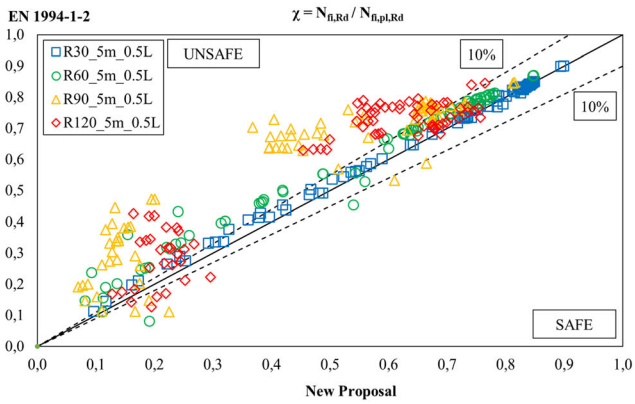

(f) Columns with 5m and 0.5L

Fig. 23 Reduction factor for PEC. Comparison between the current standard and the new proposal

5.1.4 Temperature of the reinforcing bars

The same procedure was established to determine the temperature of the reinforcing bars. It is worth mentioning that the temperature of the reinforcing bars is not directly obtained by the current version of the [4]. The resistance of the reinforcement bars under fire is obtained from calculating a coefficient that mainly depends on the geometric position of the reinforcement bars in the cross-

Table 11 Imperfection factors for buckling curves

Buckling curve	a_0	a	b	c	d
Imperfection factor α	0.13	0.21	0.34	0.49	0.76

section. Figure 16 compares the average temperature of the new proposal with the numerical results. The section factor and fire rating depict this value but also depend on its position and the geometry of the cross-section.

Figure 17shows the comparison of the average temperature of the reinforcing bars for each fire rating.

6 Comparison of Results

This section presents the comparison between the results of the current version of [4] and the new proposal. The graphs shown in Figs. 18, 19, 20 show a good agreement between the new proposal and the numerical results. For all graphs, a tolerance of 10% is presented, highlighting the safe location of the results. The difference between the current proposal for the average temperature is also noticed.

The comparison regarding the affected zone of the concrete is presented in Fig. 21 and Fig. 22. These results confirm that the residual area of concrete used to determine the load-bearing capacity is smaller when using the new proposal when compared to the current version of [4]

The 3D model results are available in the thesis developed by [33] in 2021, and were determined for two PEC lengths (3 and 5 m), for three different end conditions (pined-pined, fixed- fixed and pinned-fixed), and for the four fire ratings. Most of the numerical results presented a higher critical load when compared to results obtained from [4]. The calculation procedure may be justified this because the 3D numerical model is using all the nodal temperatures to affect the mechanical properties of every local material, while simplified methods use simplifications and average temperatures of the four components to perform the calculation. Similar comparisons, such as the elastic critical load, have been developed for intermediate results.

The relationship between the elastic critical load and the plastic resistance to axial compression is an important parameter for the design of partially encased columns (PEC) under fire, as it allows us to determinate the non-dimensional slenderness under fire. When the standard predicts a higher load-bearing resistance value than the value the structural element can withstand, the standard may be considered unsafe. The analytical and numerical results point to a smaller value of the ratio between the elastic critical load and the plastic resistance to axial compression as the fire exposure time increases. It was also observed that for PEC with the same length, 3 m or 5 m, the buckling length with different end conditions significantly affects the difference between the ratio values of the critical load and plastic resistance for the same fire exposure time. For very slender columns, buckling represents a failure mode, while for compact columns, a very high elastic critical load is required for the structural element to reach the axial force that the column can support in the imminence of buckling. Thus the plastification of the cross-section occurs long before the critical load is established. So, to ensure structural safety, reduction coefficients, and slenderness limits are applied to the structural elements in the design criteria.

The plastic resistance to axial compression is another critical parameter for designing PEC under fire. For this reason, the GMNIA was used to determine the plastic resistance of the cross-section. This procedure was used to

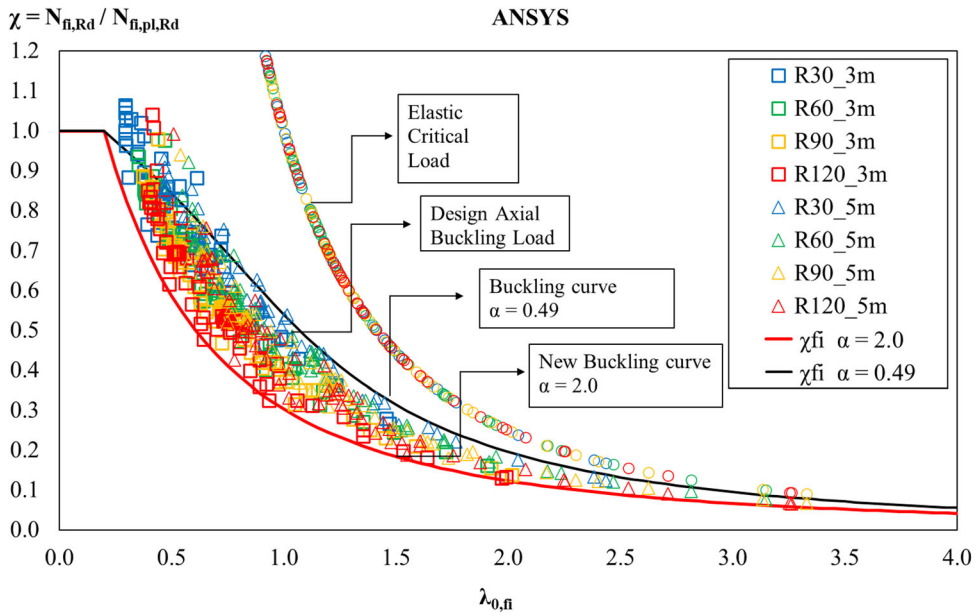

Fig. 24 Axial buckling load of PEC under fire (numerical results)

keep only results from the numerical analyses, avoiding mixing results from the simplified formulas. For this type of analysis, some considerations need to be presented to the constitutive model of the materials. The elastic-perfectly plastic model was used in the simulations for all the materials, including the concrete, assuming that part of this material is confined between the flanges.

For the axial compression in PEC, the reduction factor χ is determined for the appropriate non-dimensional slenderness λ_θ. This value depends on the buckling curve. According to the current version of the [4], curve "c" from [41] is prescribed. This reduction factor χ determines the design buckling resistance of the PEC in the fire situation. Figure 23 shows the comparison of the reduction factors when using both simplified methods ([4] and the new proposal). The results obtained from [4] are usually higher than the ones determined by the new proposal.

This difference may be justified by the improved accuracy of the new proposal to determine the correct temperature of all the components and the modifications applied to the affected zone of the concrete. Assuming that the new proposal presents accurate results, [4] presents results for some end conditions of the PEC and fire ratings, which appear unsafe.

7 Axial Buckling Load at Elevated Temperatures

The load-bearing capacity of the PEC is currently determined by the curve "c" of the Eurocode for steel structures [29]. The full 3D simulation of PEC under compressive load was developed to demonstrate the need for a different buckling curve. This section presents the results of the thermo-mechanical analysis using the GMNIA solution method. The thermo-mechanical analysis uses a steady state temperature field, determined for every fire treating time, with an incremental load step and iterative solution, based on the Newton–Raphson method. The full 3D thermal analysis extracted the temperature field after 30, 60, 90, and 120 min. Based on the first instability mode, an equivalent imperfection has been established, with a maximum amplitude of L/150. All materials involved use a perfect elastic–plastic constitutive model. Only 22 types of cross-sections are included in this part of the study, using three end conditions associated with two PEC lengths (3 and 5 m). The reduction factor due to flexural buckling under fire χ_{fi}, depends on the imperfection factor, the coefficient α, and assumes a value of 0.49. The European standard for the design of steel structures [41] admits five imperfection factors, as shown in Table 11.

Each buckling curve is assigned to calculate the reduction coefficient vχ and thus determine the design axial buckling load, depending on the cross-section classification. [4] recommends the use of the imperfection factor $\alpha = 0.49$, corresponding to the curve "c" of [41]. The numerical results reveal that curve "c" is unsafe for practically all PEC studied. Therefore, there is a need to select a new imperfection factor to adjust the buckling curve to improve the safety level of PEC under fire. According to the results presented in Fig. 24, the imperfection factor that best fits the numerical results is 2.0, see Fig. 24.

Therefore, the proposal to improve the simplified calculation method of [4] comprises new formulations to obtain the average temperatures of the four components and use an imperfection factor equal to 2.0.

8 Conclusions

The load-bearing capacity of the PEC under fire depends directly on the temperature evolution of the materials when exposed to fire. In this sense, two different solution methods were presented to determine the buckling resistance of the PEC when exposed to the standard fire [5]. This research was focused on the bucking resistance of PEC under fire, using a detailed analysis of the 2D thermal behaviour and a detailed analysis of a 3D thermo-mechanical model.

The simplified method, defined by the balance summation model, was presented using the current version of [4]. The new proposal modifies the method on the average temperature of the four components. The advanced calculation methods were validated, and a parametric analysis was developed based on 2D and 3D models.

In thefirst part of this research, a 2D model was used to present the new proposal for the balance summation model. Regarding the temperature of the flanges, the relative error of the values of the new proposal compared with the temperature determinedusing ANSYS was between + 2.5% and -2.4% for all PEC sections. The relative difference between the current proposal and the numerical results was higher, reaching values between + 11.2% and -13.0%. Regarding the web temperature, the relative difference of the new proposal values compared to those obtained by ANSYS is between + 8.8% and -12.3% for American profiles and between + 9.5% and -19.6% for European profiles. For the concrete temperatures, the relative difference of the new proposal compared to the values obtained by ANSYS was between + 5.0% and -8.9% for all PEC sections. The relative difference of the values determined by the current proposal is much higher, changing between + 29.9% and -28.4%, for all PEC sections. Concerning the reduction of the concrete layer in the direction perpendicular to the web, the relative difference

between the new proposal and the numerical results is between + 17.4% and -23.1% for all PEC sections. Despite a relatively high relative difference, the values change between + 4.4 mm and -6.2 mm. The relative differencebetween the current version of [4] and the numerical results vary between + 299.8% and -8.5%, for all PEC sections, corresponding to a difference between + 84 mm and -35.9 mm.

Regarding the reduction of the concrete layer in the web direction, the relative differencebetween the values of the new proposal and the numerical results are between + 23.9% and -15.3% for American profiles and between + 23.9% and -29.9% for all PEC sections. Again, despite a relatively high relative difference, the maximum absolute values change between + 13.1 mm and -13.8 mm. The relative difference between the current proposal of [4]and the numerical results are much higher, corresponding to + 356.8% and -16.7%, for all PEC sections, corresponding to an absolute difference between + 84 mm and -146.5 mm. For the average temperature of the reinforcing bars, the relative difference between the new proposal and the numerical results was + 14.8% and -8.1% for the American profiles and between + 14.8% and -13.6% for all PEC sections.

In the second part of this research, a full 3D analysis was developed, including non-linear thermal analysis, elastic buckling analysis and GMNIA solution methods to determine the plastic load-bearing capacity and buckling resistance of PEC under standard fire. With the 3D buckling analysis was found a new buckling curve corresponding to a different imperfection factor. It is worth noting that some simplifications of the real behaviour of a single PEC element under fire were carried out. These simplifications include the perfect contact between materials, the constitutive law of the materials, the initial equivalent imperfection and the inexistence of the thermal restraints.

Acknowledgements This study was financed by the Coordenação de Aperfeiçoamento de Pessoal de Nível Superior—Brasil (CAPES)—Finance Code 001, and by the Conselho Nacional de Desenvolvimento Científico e Tecnológico (CNPq).

Funding Coordenação de Aperfeiçoamento de Pessoal de Nível Superior,001,Ricardo A. Hoffstaeter,Conselho Nacional de Desenvolvimento Científico e Tecnológico, 001, Carlos Humberto Martins, Project n. 408498/2022-6, Brazil.

Data availability Data will be made available on request.

Declarations

Conflict of interest We have no conflicts of interest to disclose.

References

1. Simões YS, Rocha FM, Munaiar Neto J (2018) Numerical comparison between the thermostructural behavior of steel and partially coated steel and concrete composite columns in fire conditions [in Portuguese]. Revista Ibracon de Estruturas e Materiais 11(4):876–901. https://doi.org/10.1590/s1983-41952018000400012
2. Helene P, Andrade T (2010)Portland cement concrete. Chapter 29 - Civil Construction Materials and Principles of Materials Science and Engineering [in Portuguese]. Instituto Brasileiro do Concreto: IBRACON. São Paulo
3. Piquer AM, Hernández-Figueirido D (2016) Protected steel columns vs partially encased columns: fire resistance and economic considerations. J Constructional Steel Res 124:47–56. https://doi.org/10.1016/j.jcsr.2016.05.011
4. European Committee for Standardization (2005) EN 1994-1-2, Eurocode 4—design of composite steel and concrete structures - part 1–2: general rules—structural fire design. CEN, Brussels
5. International Organization for Standardization, 1999 ISO 834 - Fire-resistance tests: Elements of building construction - Part 1: General requirements for fire resistance testing. Geneva
6. Malhotra HL (1954) Effect of temperature on the crushing strength of concrete. Fire Res Stn, Boreham Wood. Engl 130:28
7. Malhotra HL, Stevens RF (1964) Fire resistance of encased steel stanchions. Proc Inst Civil Eng - ICE 29:77–98. https://doi.org/10.1680/iicep.1964.10371
8. Anderberg Y 1978 Analytical fire engineering design of reinforced concrete structures based on real fire characteristics, in Proceedings of the Eighth Congress of the Fédération Internationale de la Précontrainte, London, Concrete Society, London, pp. 112–123
9. Schleich J-B, DotreppE J-C, Franssen J-M 1986 Computer assisted analysis of the fire resistance of steel and composite concrete-steel structures. p.108. N°7210-SA/502. C.C.E, Brussels
10. Kodina K (1989) Behavior of composite columns and girders in fire. Braunschweig Fire Saf Sci 2:681–695. https://doi.org/10.3801/IAFSS.FSS.2-681
11. Lie TT, Chabot M (1990) A method to predict the fire resistance of circular steel columns filled hollow steel columns. J Fire Prot Eng 2(4):111–116
12. Maraveas C, Wang YC, Swailes T (2016) Elevated temperature behavior and fire resistance of cast iron columns. Fire Saf J 82:37–39. https://doi.org/10.1016/j.firesaf.2016.03.004
13. Winter S, Lange J 2000 Behaviour of partially encased composite columns using high-strength steel—ultimate load and fire condition. Composite Construction in Steel and Concrete IV Conference. Alberta. ASCE, p. 539–550. https://dx.doi.org/https://doi.org/10.1061/40616(281)47
14. Han L-H, Yang Y-F, Yang H, Huo J-S (2002) Residual strength of concrete-filled RHS columns after exposure to the ISO-834 standard fire. Thin-Walled Structures 40(12):991–1012. https://doi.org/10.1016/S0263-8231(02)00044-7
15. Prickett BS, Driver RG, 2006 Behavior of partially encased composite columns made with high performance concrete. Dept. of Civil and Environmental Engineering, Structural Engineering report n° 262, University of Alberta. Edmorton, p. 221. https://era.library.ualberta.ca/items/be38e47f-2a32-449c-95a7-988a515c36e5
16. Wang Z-H, Tan KH (2006) Residual area method for heat transfer analysis of concrete-encased I-sections in fire. Eng Structures 28:411–422. https://doi.org/10.1016/j.engstruct.2005.08.013
17. Correia AJMC, Rodrigues JPC (2010) Fire resistance of partially encased steel columns with restrained thermal elongation.

J Constr Steel Res 67:593–601. https://doi.org/10.1016/j.jcsr.2010.12.002
18. Ellobody E, Young B (2010) Investigation of concrete encased steel composite columns at elevated temperatures. Thin-Walled Structures 48(8):597–608. https://doi.org/10.1016/j.tws.2010.03.004
19. Korzen, M.; Rodrigues, J.P.C.; Correia, A.J.P.M. 2010 Composite Columns Made of Partially Encased Steel Sections Subjected to Fire. Structures in Fire - Proceedings of the sixth International Conference, DEStech Publications Inc, pp. 341–348. https://www.researchgate.net/publication/261438549_Composite_Columns_Made_of_Partially_Encased_Steel_Sections_Subjected_to_Fire
20. Lian SQ, Wang ZR, Wang QS, Wang L, Jiang JJ (2018) Experimental and analytical study on ultimate load capacity of RC columns in the subway stations under high-temperature gas fume effects. Int J Civil Eng 16:147–154. https://doi.org/10.1007/s40999-016-0112-4
21. Li S, Liew JYR, Xiong MX, Lai BL (2021) Experimental investigation on fire resistance of high-strength concrete encased steel composite columns". Fire Safety J. https://doi.org/10.1016/j.firesaf.2020.103273
22. Li S, Liew JYR, Xiong MX, Lai (2021) Prediction of fire resistance of concrete encased steel composite columns using artificial neural network". Eng Structures. https://doi.org/10.1016/j.engstruct.2021.112877
23. Behnam B (2018) Fire structural response of the plasco building: a preliminary investigation report. Int J Civil Eng 17:563–580. https://doi.org/10.1007/s40999-018-0332-x
24. Piloto PAG, Gavilán AB, Zipponi M, Marini A, Mesquita LMR, Plizzari G (2013) Experimental investigation of the fire resistance of partially encased beams. J Constructional Steel Res 80:121–137. https://doi.org/10.1016/j.jcsr.2012.09.013
25. Piloto PAG, Almeida David, Ramos-Gavilán Ana, Mesquita LMR 2015 Balanced summation model for the calculation of the fire resistance of partially encased steel sections: new proposals. In 6th International Conference on Mechanics and Materials in Design (M2D2015). Azores, Portugal. https://bibliotecadigital.ipb.pt/handle/10198/16717
26. Piloto PAG, Calió LJ, Rigobello R 2017 Balanced Summation model for the calculation of the buckling resistance of partially encased columns under fire: new improvements.Proceedings of Research and advanced technology in fire safety, University of Santander - GIDAI, Santander, Spain. p. 271–287, https://bibliotecadigital.ipb.pt/bitstream/10198/21737/1/REF_202_2017_FIRESAFETY_2017_proceedings_full_paper_pen_drive_01_PPILOTO.pdf
27. Piloto PAG, Alfredo BF, Rossetto DR 2018 Partially encased columns: strength and stiffness effect on the buckling resistance under fire. 6th Conference on Urban Fire Safety and 1st Civil Protection Conference. https://bibliotecadigital.ipb.pt/handle/10198/21698
28. Fellouh A, Bougara A, Piloto P, Benlakehal N (2022) Fire resistance of partially encased composite columns subjected to eccentric loading. J Structural Fire Eng 13(4):451–469. https://doi.org/10.1108/JSFE-09-2021-0057
29. European Committee for Standardization (2005) EN 1993-1-2, Eurocode 3 - design of steel structures - part 1–2: general rules - structural fire design. European Standards, Brussels
30. European Committee for Standardization (2004) EN 1992-1-2, Eurocode 2 - Design of concrete structures - part 1–2: general rules – structural fire design. European Standards, Brussels
31. Jungbluth O (1982) Optimierte verbundbauteile. Stahlbau Verlags GmbH, Köeln
32. European Committee for Standardization, 2002 EN 1991–1–2, Eurocode 1: Actions on structures – Part 1–2: General actions – Actions on structures exposed to fire, CEN- European Committee for Standardization. CEN- European Committee for Standardization, Brussels, p. 59
33. Hoffstaeter, R. A. 2021 Análise do comportamento de pilares mistos parcialmente revestidos em situação de incêndio, http://www.pcv.uem.br/documentos/dissertacao-de-mestrado/ricardo hoffstaeter-pdf.pdf, [in Portuguese], Paraná, Brazil.
34. Stefan R, Sura J, Procházka J, Kohoutková A (2019) Wald, F. Numerical investigation of slender reinforced concrete and steel-concrete composite columns at normal and high temperatures using sectional analysis and moment-curvature approach. Eng Struct 190:285–305. https://doi.org/10.1016/j.engstruct.2019.03.071
35. HAß, Rüdiger. 1986 Zur praxisgerechten brandschutztechnischen Beurteilung von Stützen aus Stahl und Beton. https://doi.org/10.24355/dbbs.084-201310181517-0
36. Piloto PAG, Ramos A, Gonçalves C, Mesquita L (2017) Experimental bending tests of partially encased beams at elevated temperatures. Fire Saf J 92:23–41. https://doi.org/10.1016/j.firesaf.2017.05.014
37. Rocha A, FM 2016 Pilares de Aço e Mistos de Aço e Concreto Inseridos em Paredes em Situação de Incêndio. 2016 Doutorado em Engenharia de Estruturas, Universidade de São Paulo. São Carlos, Brasil. Universidade de Coimbra, Portugal, http://repositorio.eesc.usp.br/handle/RIEESC/5285
38. Simões YS, Rocha FM, Munair Neto J (2018) Comparação numérica entre o comportamento termoestrutural de pilares de aço e mistos de aço e concreto parcialmente revestidos em situação de incêndio. Revista Ibracon de Estruturas e Materiais 11(4):876–901. https://doi.org/10.1590/s1983-41952018000400012
39. Correia AJMC, Rodrigues JPC (2010) Fire resistance of partially encased steel columns with restrained thermal elongation. J Constructional Steel Res 67:593–601. https://doi.org/10.1016/j.jcsr.2010.12.002
40. British Standard Institution. BSI. EN 1363–1:2012. 2020 Fire resistance tests – Part 1: General Requirements. London: BSI
41. European Committee for Standardization (2005) EN 1993-1-1, Eurocode 3 - design of steel structures - part 1–1: general rules – rules for buildings. European Standards, Brussels